creative commons
COMMONS DEED

저작자표시-비영리-변경금지 2.0 대한민국

이용자는 아래의 조건을 따르는 경우에 한하여 자유롭게

- 이 저작물을 복제, 배포, 전송, 전시, 공연 및 방송할 수 있습니다.

다음과 같은 조건을 따라야 합니다:

저작자표시. 귀하는 원저작자를 표시하여야 합니다.

비영리. 귀하는 이 저작물을 영리 목적으로 이용할 수 없습니다.

변경금지. 귀하는 이 저작물을 개작, 변형 또는 가공할 수 없습니다.

- 귀하는, 이 저작물의 재이용이나 배포의 경우, 이 저작물에 적용된 이용허락조건을 명확하게 나타내어야 합니다.
- 저작권자로부터 별도의 허가를 받으면 이러한 조건들은 적용되지 않습니다.

저작권법에 따른 이용자의 권리는 위의 내용에 의하여 영향을 받지 않습니다.

이것은 이용허락규약(Legal Code)을 이해하기 쉽게 요약한 것입니다.

Disclaimer

dCollection

조선대학교
CHOSUN UNIVERSITY

2022년 2월
석사학위 논문

pH-universal Electrocatalyst based on Ultralow Amount of Ruthenium through Selective Deposition for Hydrogen Evolution Reaction

조 선 대 학 교 대 학 원

화 학 공 학 과

정 예 빈

조선대학교
CHOSUN UNIVERSITY

pH-universal Electrocatalyst based on Ultralow Amount of Ruthenium through Selective Deposition for Hydrogen Evolution Reaction

선택적인 증착을 통해 극소량의 루테늄을 기반으로 한 pH-universal 수소 생성 반응 전기촉매

2022년 2월 25일

조 선 대 학 교 대 학 원

화 학 공 학 과

정 예 빈

조선대학교
CHOSUN UNIVERSITY

pH-universal Electrocatalyst based on Ultralow Amount of Ruthenium through Selective Deposition for Hydrogen Evolution Reaction

지 도 교 수　　안 성 훈

이 논문을 공학 석사학위신청 논문으로 제출함

2021년 10월

조 선 대 학 교　대 학 원

화 학 공 학 과

정　　예　　빈

조선대학교
CHOSUN UNIVERSITY

정예빈의 석사학위논문을 인준함

위 원 장 조선대학교 교 수 이 중 헌 (인)

위 원 조선대학교 교 수 이 정 수 (인)

위 원 조선대학교 교 수 안 성 훈 (인)

2021년 12월

조 선 대 학 교 대 학 원

조선대학교
CHOSUN UNIVERSITY

C O N T E N T S

조선대학교
CHOSUN UNIVERSITY

조선대학교
CHOSUN UNIVERSITY

List of Tables

조선대학교
CHOSUN UNIVERSITY

List of Figures

조선대학교
CHOSUN UNIVERSITY

조선대학교
CHOSUN UNIVERSITY

조선대학교
CHOSUN UNIVERSITY

조선대학교
CHOSUN UNIVERSITY

조선대학교
CHOSUN UNIVERSITY

ABSTRACT

선택적인 증착을 통해 극소량의 루테늄을 기반으로 한 pH-universal 수소 생성 반응 전기촉매

Jeong, Ye bin
Advisor : Prof. Ahn, Sung-hoon, Ph.D.
Department of Chemical Engineering,
Graduate School of Chosun University

수소 생성 반응에 대해 효율적이고 경제적인 전기 촉매의 개발은 전기화학적 방법에서 가장 현실적이고 중요한 과제이다. 본 연구에서는 템플릿 역할을 할 수 있는 멤브레인을 제작해 다른 기질을 추가적으로 사용하지 않는 freestanding monolith를 제작했다. 이후 코발트를 도입하여 단일 원자 상태의 Co-N-C 결합을 형성하고, 최종적으로 루테늄 나노입자를 탄소 매트릭스 표면에 증착하여 pH-universal 수소 생성 반응 전기촉매를 개발한다.

전이금속 (Fe, Co, Ni, Mo)은 전기촉매 분야에서 활발하게 연구되고 있는 재료로서, 공정을 통해 Co-N-C를 형성하게 되며 이는 촉매의 활성점으로 작용하여 성능을 향상하는데 도움을 준다. 또한 루테늄을 모노리스 촉매 표면에 선택적으로 증착하여 극소량의 루테늄만으로도 촉매 성능을 극대화시켜 벤치마크 전극인 상용 Pt/C에 견줄만한 결과를 나타낼 수 있다. 제작된 CoSA-N-C@Ru 전기촉매는 염기성 전해질에서 10 mA cm^{-2}의 전류밀도를 달성하기 위해 오직 14 mV만의 과전압을 필요로 하며 산성 전해질에서는 11 mV의 과전압을 필요로 해 수소 생성 반응에 대해 우수한 촉매활동을 보여준다. 또한 내구성 시험을 통해 100시간 이상의 시험에도 성능이 그대로 유지되어 우수한 내구성을 보인다.

조선대학교
CHOSUN UNIVERSITY

컨트롤 샘플을 이용하여 진행한 실험 결과와 비교해 보았을 때 두 가지 중요한 주목할 만 한 점을 발견했다. 우선 코발트가 응집되지 않고 단일 원자 상태로 존재할 때 수소 생성 반응에 대한 성능이 가장 좋다는 것을 확인할 수 있다. 다음으로, 반응하는 루테늄의 양에 비례하여 수소 생성 반응에 대한 성능이 확연하게 증가하지 않는다는 점이다. 이 결과와 함께 최종적으로 본 연구에서는 전이금속 단일 원자와 귀금속 나노입자의 조합과 함께 HER 촉매의 가능성을 제안한다.

Keywords: pH-universal, selective deposition, electrocatalyst, free-standing, hydrogen evolution reaction

조선대학교
CHOSUN UNIVERSITY

I. Introduction

A. Background of study

As the limited resources such as fossil fuels, coals are decreasing and the global warming is increasingly severe, the new energy sources need to be developed to replace conventional resources. Hydrogen energy has a high energy density and because it does not generate carbon dioxide when combustion, it is attracting much attention as an alternative to fossil fuel. It can also store energy in the form of hydrogen, enabling continuous energy use [1-3]. When hydrogen is produced through electrochemical water splitting, it is a simple process and can obtain clean hydrogen, but the most important thing is the development of high performance electrocatalysts. The Pt-based electrocatalysts used in overall water splitting are known to show the excellent activity toward hydrogen evolution reaction (HER) in both acidic and alkaline condition [4-6]. However, Pt has many difficulties in commercializing as an water splitting electrocatalyst due to its limited amount of available resources, and most of all, its high price [7]. So many studies are trying to produce Pt-free electrocatalysts which has a performance comparable to Pt. Many studies are underway on transition metals (Fe [8], Co [9], Ni [10], Mo [11]) based electrocatalysts to replace Pt, but due to its energy barriers, most of them do not exhibit Pt-like performance especially in alkaline electrolytes. Therefore, the development of electrode materials that can show high activity comparable to Pt in both acidic and alkaline electrolytes is the most important and essential now.

Introducing small amount of noble metals is one of the promising ways to improve catalytic performance toward hydrogen production [12]. Noble metals such as Ru [13], Rh [14], and Ir [15], which are included in the Pt group, have received much attention for their HER performance. In particular, the aforementioned obstacle, HER activity in alkaline electrolytes can also be improved, which is expected to be an effective electrode material to replace Pt. Therefore, by introducing noble metals to transition metal based materials, it can reduce the loading of noble metals, making them more inexpensive and improving catalytic performance and durability [16,17]. Currently, several Ru-based catalytic materials such as Ru oxide, Ru nanoparticles, and Ru alloys

조선대학교
CHOSUN UNIVERSITY

are being studied as the high-performance electrocatalysts [16,18].

But the price of Ru is still expensive compared to other non-noble metals although it is more inexpensive than Pt. The most promising way to decrease in the loading of Ru is to reduce the size of Ru nanoparticles, minimizing the inaccessible active sites to HER.

Herein, we developed a method of reducing the loading amount of Ru and improving the performance toward HER through the selective deposition of Ru onto the as-prepared carbon monolithic membrane. Firstly, the fibrous carbon membrane coated with bimetallic ZIFs containing Zn and Co is fabricated to be used as the sacrificial templates. Through the annealing process, the Zn species evaporate to form meso/macropores and the Co-N-C active sites are generated. Next, the highly porous fibrous carbon membrane reacts with the aqueous solution containing $RuCl_3$, which deposit uniformly into the pre-existing pores of the carbon fibers. It is noteworthy that the HER activity is similar to that of commercial Pt/C, in both alkaline and acidic electrolyte. In alkaline condition, CoSA-N-C@Ru requires only 14 mV of overpotential to achieve 10 mA cm^{-2}, almost similar to that of commercial Pt/C ($\eta_{j=10}$ of 24 mV). Likewise, in acidic condition, CoSA-N-C@Ru requires 11 mV and Pt/C requires 7 mV of overpotential, indicating the highly efficient pH-universal electrocatalyst. The results by two control experiments show that when Co exists in isolated single atomic state, it can react with a ultralow amount of Ru. Furthermore, in the second control experiment, all conditions were equivalent and only the reacting amount of Ru was controlled to verify HER performance, and the experiment demonstrated that a small amount of Ru has no significant effect on HER performance.

조선대학교
CHOSUN UNIVERSITY

B. Background of experiment

1. Ruthenium

Metals such as Rh, Ru, and Ir which are included in the Pt group have received much attention for their HER performance, which is more inexpensive than Pt but is similar or superior to Pt [13-15]. In the reported literatures, the metallic Ru can be uniformly dispersed in various carbon supports. In addition, when Ru species are introduced into nitrogen-doped carbon, it exhibits good pH-universal activity toward HER process in both alkaline and acidic electrolytes [16,19]. Likewise, it is known that the introduction of transition metals to generate Ru-M (M is transition metal such as Ni, Co and Fe) into the carbon matrix improves HER activity [16,17]. In particular, in an alkaline electrolyte, the Ru-based electrocatalysts had better HER activity than Pt/C because the energy barrier toward water splitting was insignificant. Thus, several recently reported literatures on these bimetallic materials with nitrogen-doped carbon matrix showed high pH-universal HER activity.

Although the price of Ru is more inexpensive than Pt, it is still expensive compared to the other non-noble metal species. The most promising method to decrease the loading amount of Ru is to reduce the size of particles, minimizing the proportion of inaccessible active sites and exposing Ru-based accessible active sites to stimulate HER activity [20,21]. In particular, Ru is evenly dispersed in the carbon matrix and coordinates with carbon or nitrogen to form a Ru-Nx active site. To date, the coexistence of metallic Ru nanoparticles and a single atomic Ru-Nx active site is helpful in pH-universal HER activity due to the synergistic effect between nanoparticles/clusters and single atoms [22].

조선대학교
CHOSUN UNIVERSITY

2. Metal organic framework

Metal organic frameworks (MOFs) is a structure composed of metal and organic ligand. MOFs have a high surface area, porosity, and many active sites that have been applied in many fields, including catalysts, gas adsorption, and sensors [23,24]. Many researchers have now reported a number of MOFs synthesized based on various combinations of metal ions and organic ligand. MOFs can be activated through chemical treatments and can be used as precursors of electrode materials. The active site of MOFs generated by the aforementioned activations helps to improve the HER performance of electrode materials [25,26].

조선대학교
CHOSUN UNIVERSITY

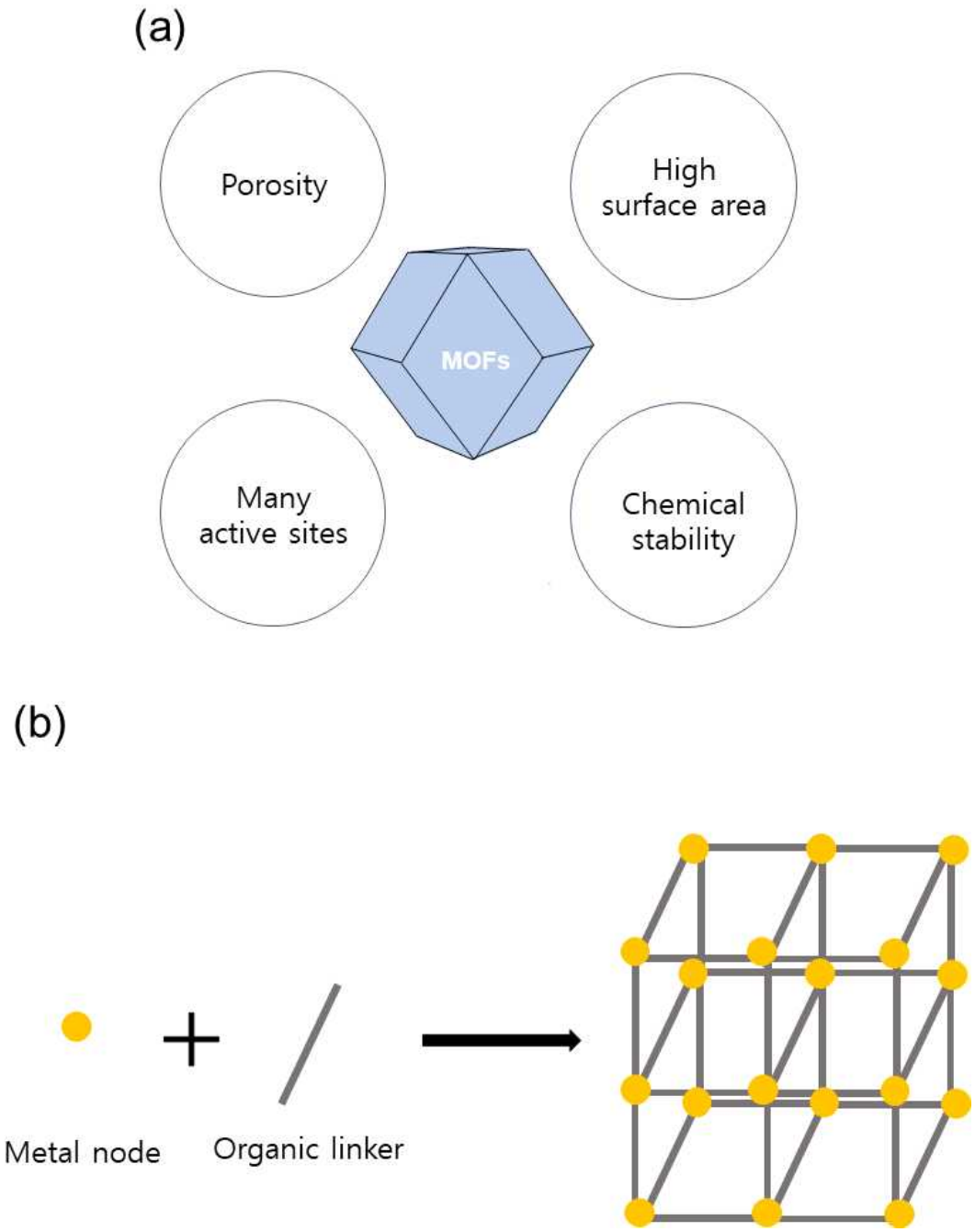

Figure 1. Illustration of the (a) characterization and (b) structure of MOFs.

조선대학교
CHOSUN UNIVERSITY

3. Hydrogen evolution reaction

The overall electrochemical water splitting which is the clean and simple process consists of two half- reaction: hydrogen evolution reaction (HER) and oxygen evolution reaction (OER). To develop the efficient electrocatalyst that can reduce the energy barrier during the hydrogen production is important. The HER mechanism is related to the hydrogen adsorption/desorption reaction occuring on the surface of the catalytic electrode [4,8,12]. In the volcano plot which indicates that the adsorption/desorption energy value of metal species, the adsorption/desorption energy is lower than that of Pt which means the ability to produce hydrogen efficiently. In both alkaline and acidic electrolytes, through Volmer-Tafel mechanism or Volmer-Heyrovsky mechanism, the hydrogen is produced by water splitting [13,27].

조선대학교
CHOSUN UNIVERSITY

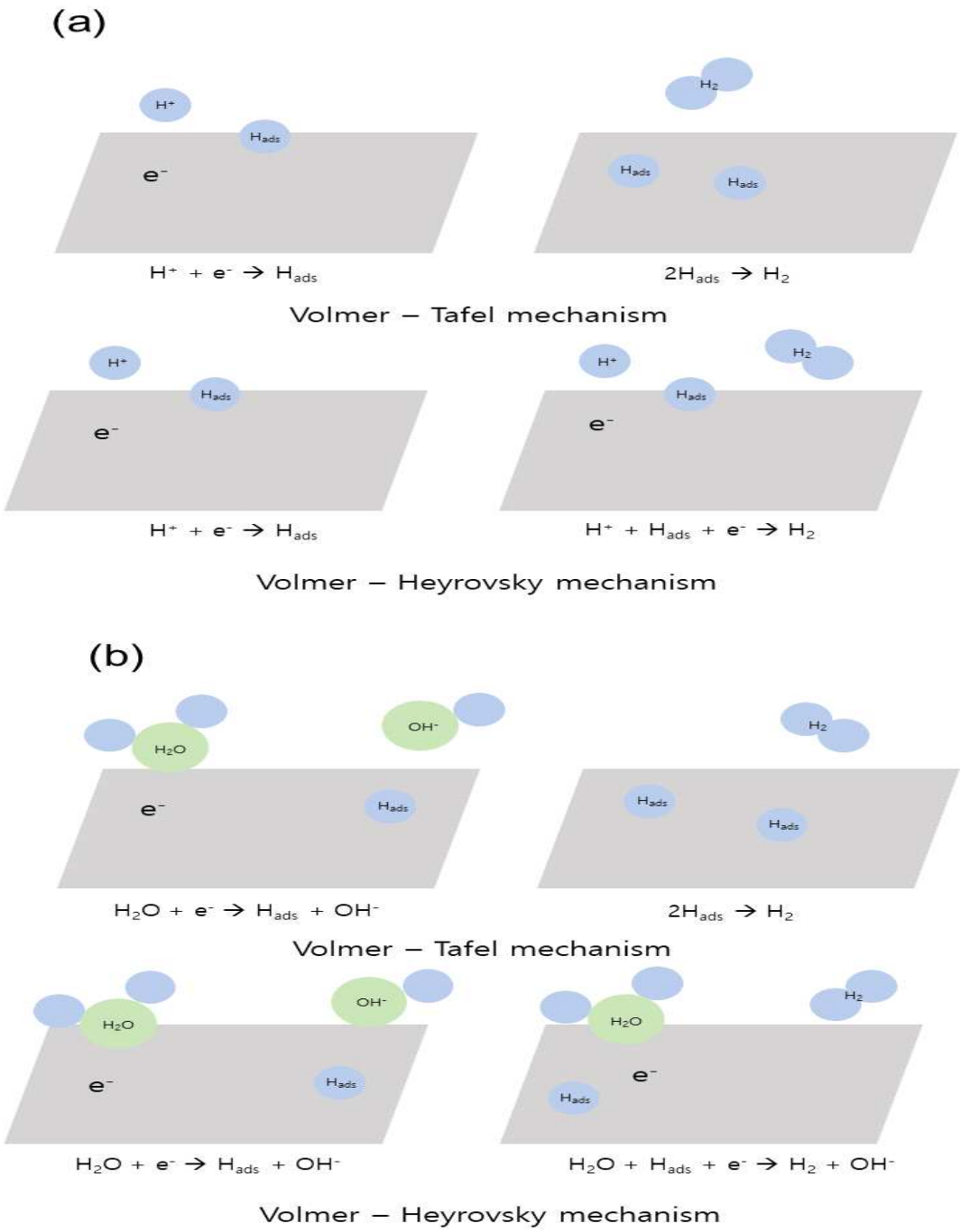

Figure 2. Illustration of HER process of Volmer-Tafel mechanism and Volmer-Heyrovsky mechanism (a) in an acidic electrolyte and (b) in an alkaline electrolyte.

조선대학교
CHOSUN UNIVERSITY

II. Experimental section

A. Synthesis of monolithic CoSA-N-C@Ru electrode

1. Synthesis of fibrous CoSA-N-C freestanding membrane

1.44 g of tellurium (IV) oxide (TeO_2) and 1.8 g polyvinyl pyrrolidone (PVP) were dissolved in 150 ml of ethylene glycol and stirred at 200 °C. When the solution became colorless, 0.9 g of sodium hydroxide was added and kept for 25 minutes. The tellurium nanowires were obtained by vacuum-filtration, and re-dispersed into 200 ml of methanol. And then, 5.8 mmol of zinc nitrate hexahydrate ($Zn(NO_3)_2{\cdot}6H_2O$), 2.5 mmol of cobalt (II) nitrate hexahydrate ($Co(NO_3)_2{\cdot}6H_2O$) and 14.6 mmol of 2-methylimidazole (2MI) were added into above tellurium nanowires solution. The solution was magnetically stirred overnight and collected by vacuum-filtration to obtain freestanding ZIFs-derived membrane. The ZnCo-ZIFs monolithic membrane was dried at room temperature. The ZnCo-ZIFs membrane were placed into an alumina oxide crucible, and loaded into tube furnace. By an annealing process, ZnCo-ZIFs was converted into nitrogen-doped carbon matrix with cobalt single atoms (CoSA-N-C) under argon flow at 950 °C for 6 hours at a ramping rate of 5 °C min^{-1}, and cooled down to room temperature naturally. As the control group, nitrogen-doped carbon with cobalt nanoparticles (CoNPs-N-C) and Co-free sample (N-C) were prepared by controlling the molar ratio of zinc and cobalt.

2. Synthesis of CoSA-N-C@Ru with ultralow loading of Ru

As-prepared four pieces of CoSA-N-C membrane were immersed into 13.25 aqueous solution containing 0.25 ml of ruthenium(III) chloride hydrate ($RuCl_3{\cdot}xH_2O$) solution (30 mg ml^{-1}). The solution was magnetically stirred at 70 °C and kept for 16 hours. After this process, the products were washed with ethanol, and finally dried at room temperature. The obtained CoSA-N-C@Ru monolithic electrodes were used as the catalytic electrode without any further treatment. As the control group, the amount of $RuCl_3$ solution was controlled from 0.1 ml to 5.0 ml (denoted as CoSA-N-C@Ru-X, and X is amount of solution containing $RuCl_3$ precursor).

조선대학교
CHOSUN UNIVERSITY

3. Electrochemical measurement

The electrochemical measurements were analyzed with bi-potentiostat workstation. The HER electrochemical analysis was executed with three-electrode configuration. In an alkaline condition, 1 M KOH was used as an electrolyte, and mercurous oxide electrode (Hg/HgO with 1 M NaOH solution) and a platinum wire were used as the reference, and counter electrode, respectively. In an acidic condition, 0.5 M H_2SO_4 was used as an electrolyte, and saturated calomel electrode (SCE with saturated KCl solution) and a graphite rod or Ir/C were used as the reference, and counter electrode, respectively. Both an alkaline and acidic condition, the as-prepared monolithic catalyst was used as the working electrode. The measured potential with reference mercurous oxide and saturated calomel electrode were converted to potential of reversible hydrogen electrode (V_{RHE}) by the following equation.

$$V_{RHE} = V_{Hg/HgO} + (0.14+0.059*pH)V \text{ in alkaline condition}$$
$$V_{RHE} = V_{SCE} + (0.244+0.059*pH)V \text{ in acidic condition}$$

Each linear sweep voltammetry (LSV) measurement was executed after stabilization of 50 cycles with a potential range of -0.4 to 0.05 V_{RHE}. Nyquist plots were obtained by EIS analysis with frequency range of 10^6 to 10^{-1} Hz with an amplitude perturbation of 5 mV. LSV curves were obtained with a scan rate of 0.1 mV s^{-1} with 100% iR compensation. For the durability test, cyclic voltammetry (CV) measurement was performed with a 100 mV s^{-1} of sweep rate for 10,000 times in alkaline and acidic electrolytes. The chronoamperometric test was executed with a 10 mA cm^{-2} of current density in alkaline and acidic electrolytes.

조선대학교
CHOSUN UNIVERSITY

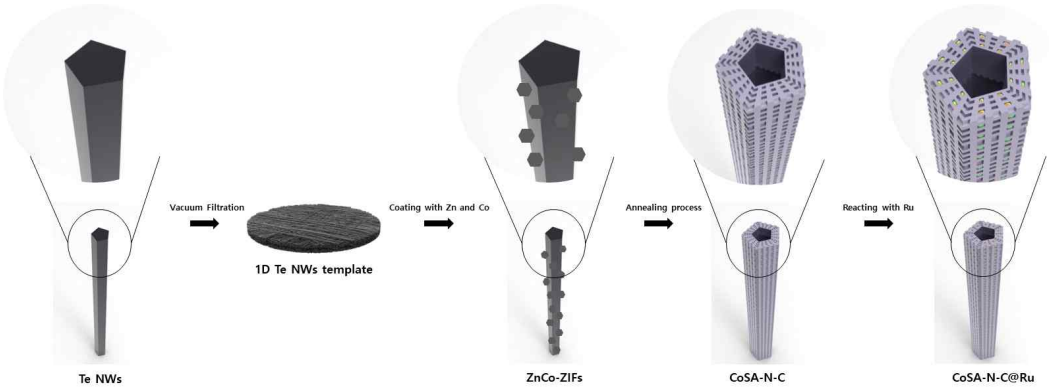

Figure 3. The overall process of fabrication of CoSA-N-C@Ru.

조선대학교
CHOSUN UNIVERSITY

III. Results and Discussion

A. The structure characterization of highly porous monolith CoSA-N-C@Ru electrode

The synthesis method of CoSA-N-C@Ru is schematically illustrated in Figure 4. First, one-dimensional Te nanowires (Te NWs) are fabricated as the sacrificial template [28]. And the bimetallic ZIFs containing Zn and Co with varied molar ratio are coated on the surface of Te NWs, and the as-prepared ZnCo-ZIFs was collected by vacuum-filtration to form a freestanding membrane which has about 3.7 cm of diameter (Figure 5a-b). The ZnCo-ZIFs membrane was cut to 1 cm X 1 cm in several pieces, and through annealing process, a ZnCo-ZIFs was converted to cobalt-nitrogen-carbon (Co-N-C) matrix (Figure 5c) and Zn species were evaporated to form the porous structure. When the molar ratio of Zn and Co with 7:3 was selected, embedded single atomic Co in N-doped carbon (CoSA-N-C) was created without nanocluster/nanoparticle Co. The formation of porous structure of CoSA-N-C promotes to deposit Ru onto the surface of macro/nanopores of carbon matrix.

Through the following process, being immersed in a solution containing the Ru precursor, Ru species were deposited onto the porous carbon fibers. The cut monolithic CoSA-N-C pieces were immersed in aqueous solution containing $RuCl_3$ (30 mg ml^{-1}). The molar ratio of Zn and Co and the amount of Ru were adjusted to investigate the effect of size of Co and Ru. In this study, the strategy of selective and direct deposition of Ru on the freestanding porous carbon matrix achieves high HER performance. In previously reported literatures, the reaction of an aqueous solution containing Ru on the powdery carbon catalyst is feasible to deposit uniformly, but it leads to a relatively high loading amount of Ru [29,30]. In addition, the powdery catalyst is stacked to form a dense layer, makes the active site inaccessible. In contrast, when Ru is deposited on the monolithic carbon catalyst, the Ru species are deposited only in an accessible site, thereby forms a catalyst with a trace amount of Ru. This selective deposition at the active sites limits the formation of inaccessible active sites.

조선대학교
CHOSUN UNIVERSITY

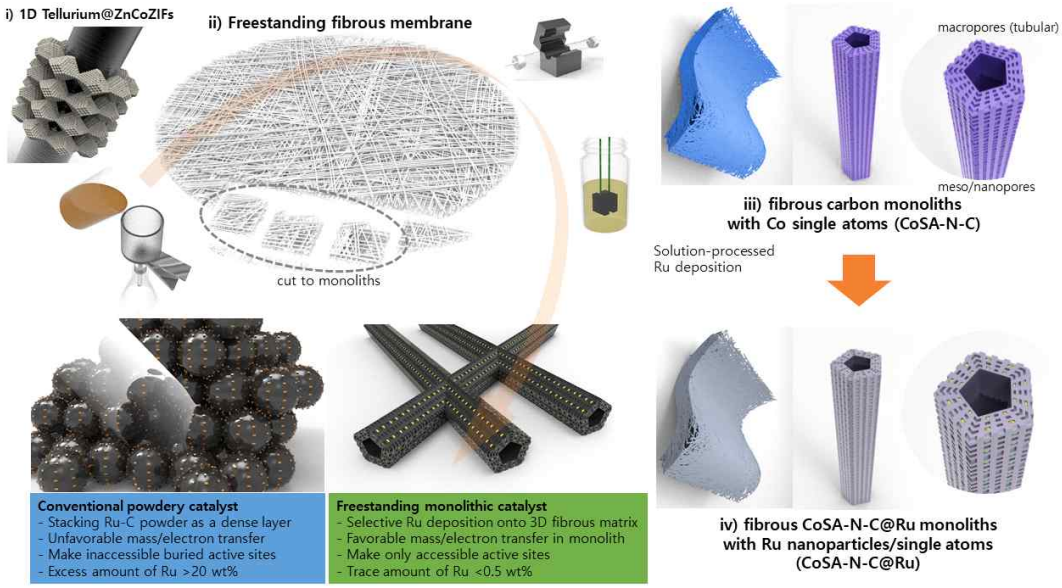

Figure 4. Schematic illustration of the preparation of freestanding monolith CoSA-N-C@Ru catalytic electrode.

조선대학교
CHOSUN UNIVERSITY

Before the fabrication of the CoSA-N-C@Ru, the nanostructures of Te NWs and ZnCo-ZIFs were observed by field-emission scanning electron microscope (FE-SEM). In Figure 5, the first produced Te NWs consist of fibers with a relatively smooth surface, and are well interconnected with an average diameter of 100 nm. This nanowire structure is used as a template for the final catalytic electrode. Next, nanowires coated uniformly with bimetallic ZIFs including Zn and Co, have a much more porous and rough surface than Te NWs (Figure 6). This ZnCo-ZIFs is used as a sacrificial template for maintaining the structure and being deposited by metal in a subsequent annealing process. The vacuum-filtrated ZnCo-ZIFs monolithic membrane with 3.7 cm of diameter is shown in Figure 7.

Through the subsequent annealing process, one dimensional porous carbon fibers with single atomic Co were observed by the top view SEM images in Figure 8a-c. These fibrous nanowires are well interconnected and self-assembled, and create freestanding monolith that do not require other additional substrates. Differently with ZnCo-ZIFs, as Zn evaporated during the annealing process, meso/nanopores were generated in the pre-existing ZIF structure, and metallic Co was not observed. In order to study the effect of Co size in this fibrous carbon matrix, the molar ratio of Zn and Co was adjusted to Co-free (ZnCo 10:0), Zn-rich (ZnCo 9:1), equivalent (ZnCo 5:5), Co-rich (ZnCo 3:7), and Zn-free (ZnCo 0:10). As shown in the Figure 9, similar morphology was observed of Co-free and Zn-rich N-C, and no additional Co nanoparticles were observed. On the other hand, in the Figure 10 and Figure 11, it was confirmed that at molar ratio of Zn and Co is 5;5, 3:7, and 0:10, which have a high Co ratio, the Co nanoparticles increased.

In the tilted view SEM images of Figure 8d-e, after selective deposition of Ru on fibrous carbon membrane, the monolithic carbon matrix does not have any cracks and is well-connected with an average height of 310 μm. Carbon fibers observed in the top view SEM images maintained the porous structure well even after the deposition of Ru, and very small Ru nanoparticles, marked by white circles in the Figure 8g could be observed in high-resolution SEM. For comparison, the amount of Ru solution was adjusted to confirm CoSA-N-C@Ru-X (X is amount of Ru solution) produced using 0.1 ml, 0.5 ml, 1.0 ml, and 5.0 ml of Ru solution. Ru nanoparticles were not observed in

조선대학교
CHOSUN UNIVERSITY

CoSA-N-C@Ru-0.1 in the Figuer 12 a-b, whereas in Figure 12 c-d and e-f, CoSA-N-C@Ru-0.5 and CoSA-N-C@Ru-1.0 had larger Ru nanoparticles than CoSA-N-C@Ru (Ru 0.25 ml). It is notable that when reacting with excessive Ru solution, Ru nanosheets are formed on carbon fibers as shown in Figure 13.

조선대학교
CHOSUN UNIVERSITY

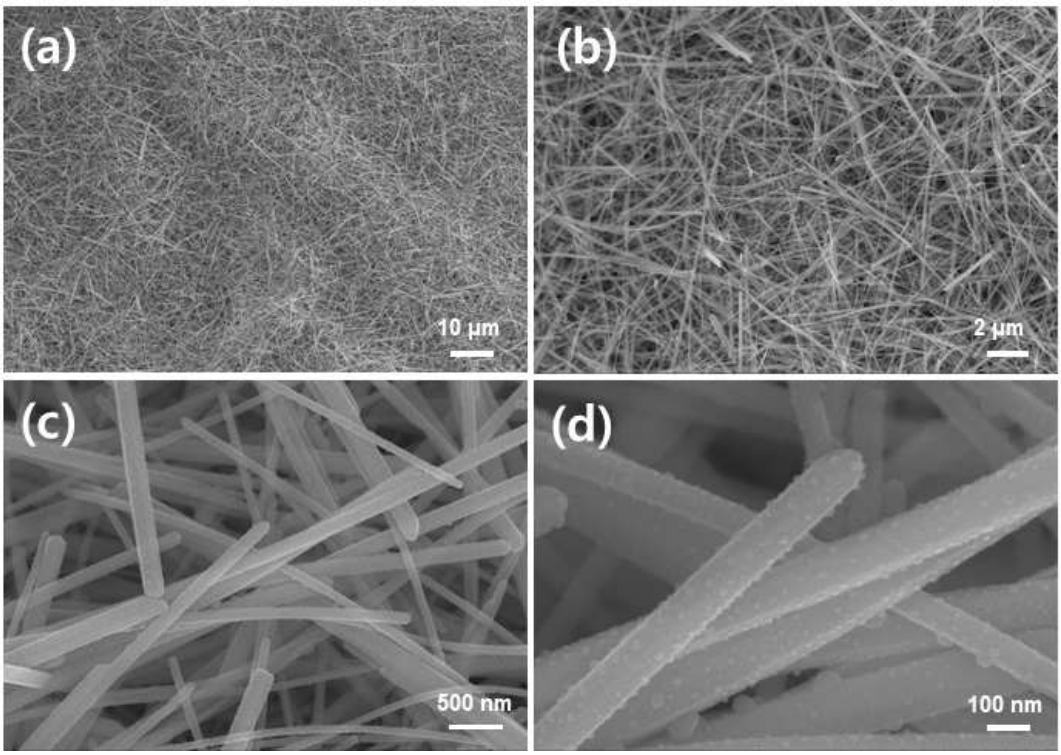

Figure 5. (a-d) SEM images of tellurium nanowires.

조선대학교
CHOSUN UNIVERSITY

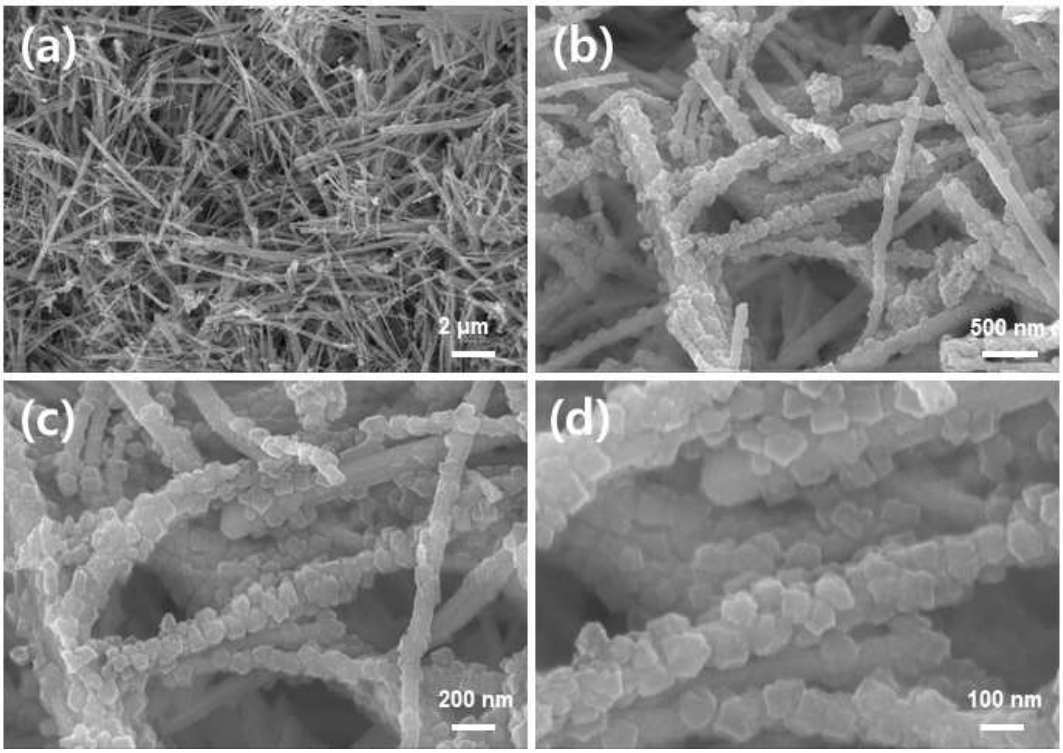

Figure 6. (a-d) SEM images of ZnCo-ZIFs.

조선대학교
CHOSUN UNIVERSITY

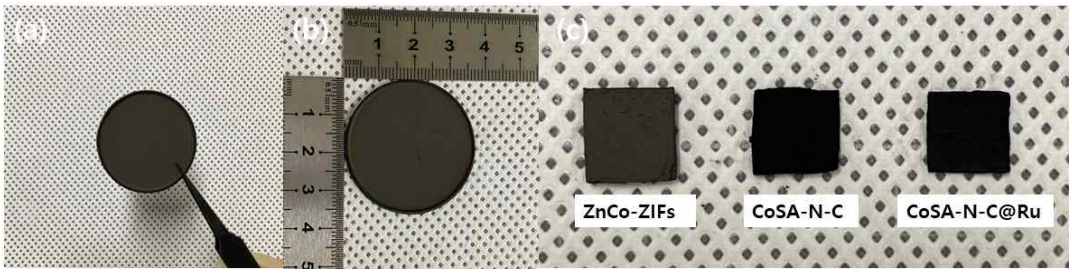

Figure 7. Photograph images of (a,b) ZnCo-ZIFs membrane, (c) pieces of monoliths cut to 1 cm^{-2}.

조선대학교
CHOSUN UNIVERSITY

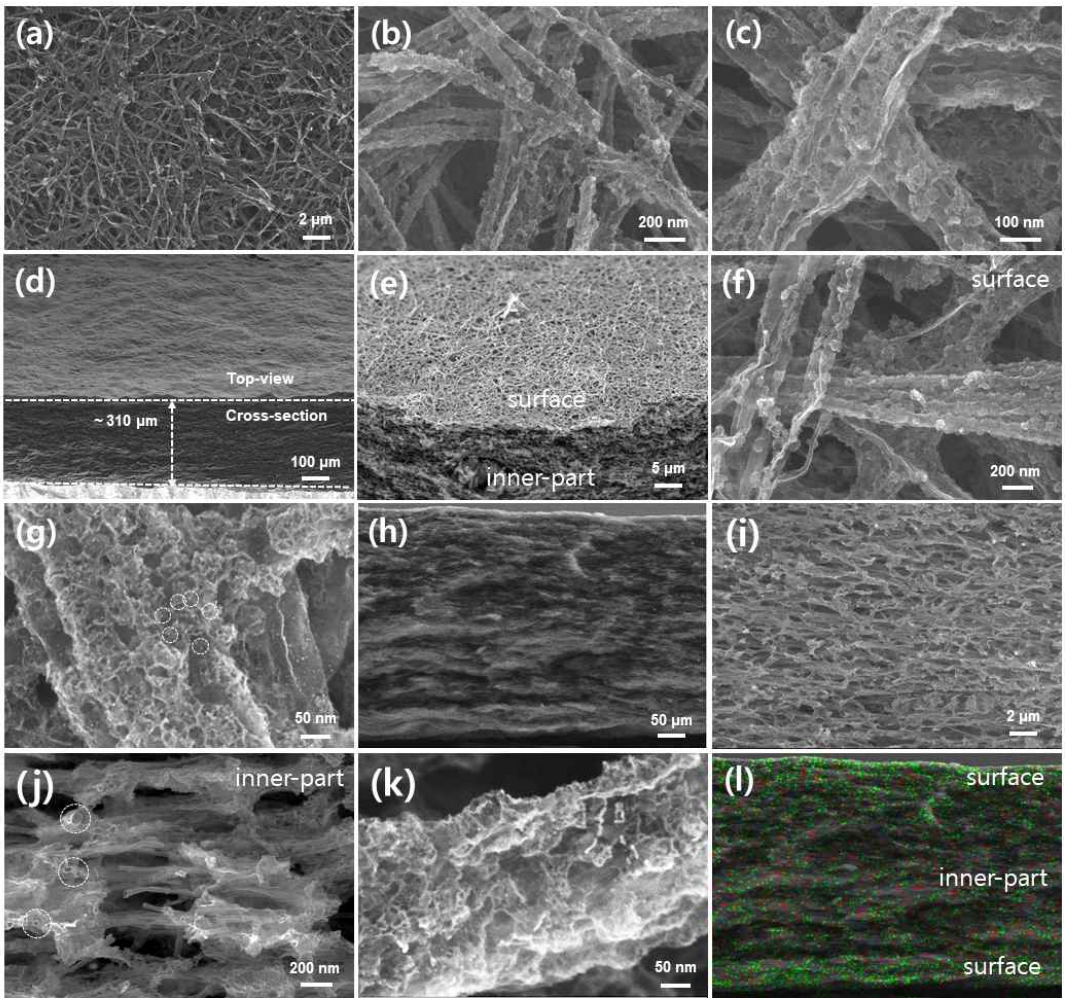

Figure 8. SEM images of (a-c) CoSA-N-C. (d,e) Tilted view, (f,g) top-view and (h-k) cross-section SEM inages of CoSA-N-C@Ru. (l) corresponding EDX image of Ru and Co elements.

조선대학교
CHOSUN UNIVERSITY

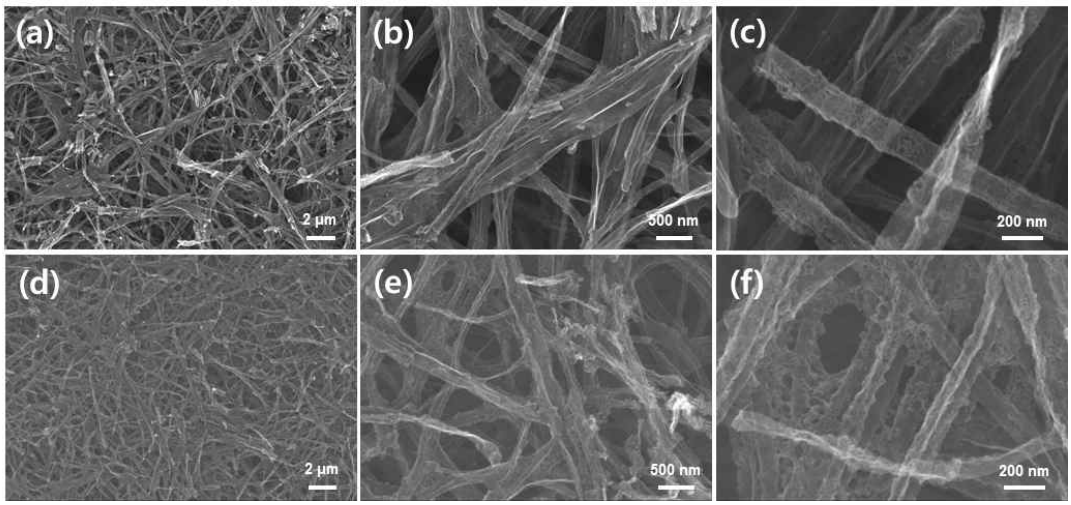

Figure 9. SEM images of bimetallic ZnCo ZIFs-derived monolithic fibers with a molar ratio of Zn:Co with (a-c) 10:0, (d-f) 9:1.

조선대학교
CHOSUN UNIVERSITY

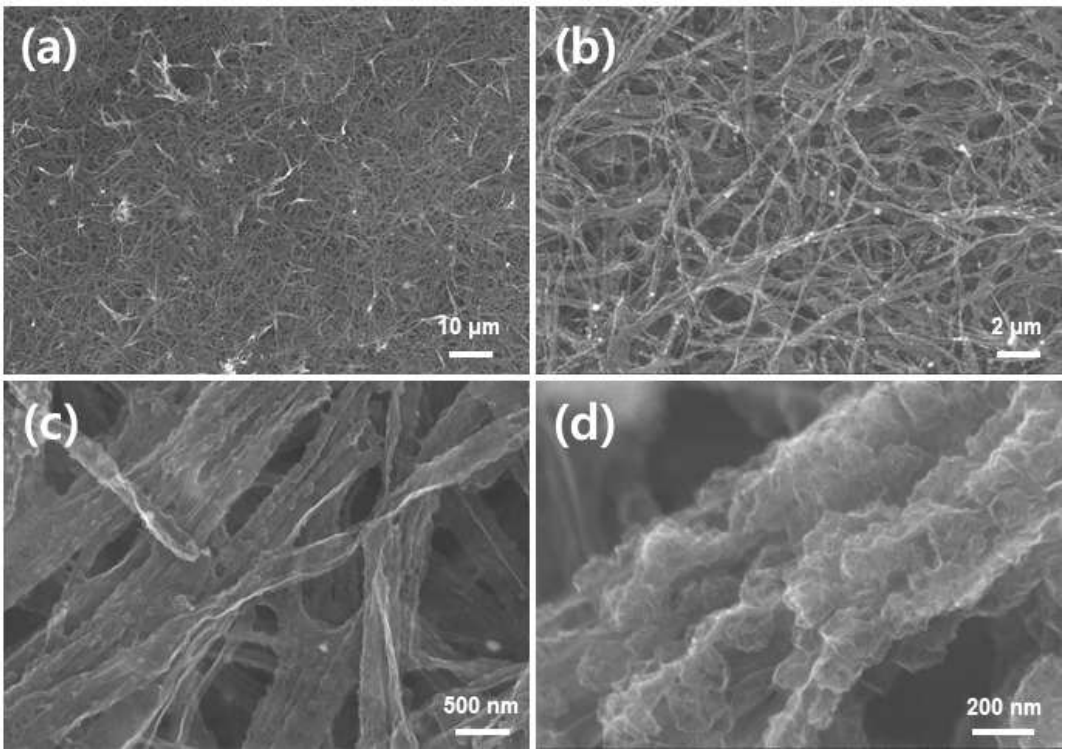

Figure 10. (a-d) SEM images of bimetallic ZnCo ZIFs-derived monolithic fibers with a molar ratio of Zn:Co with 5:5.

조선대학교
CHOSUN UNIVERSITY

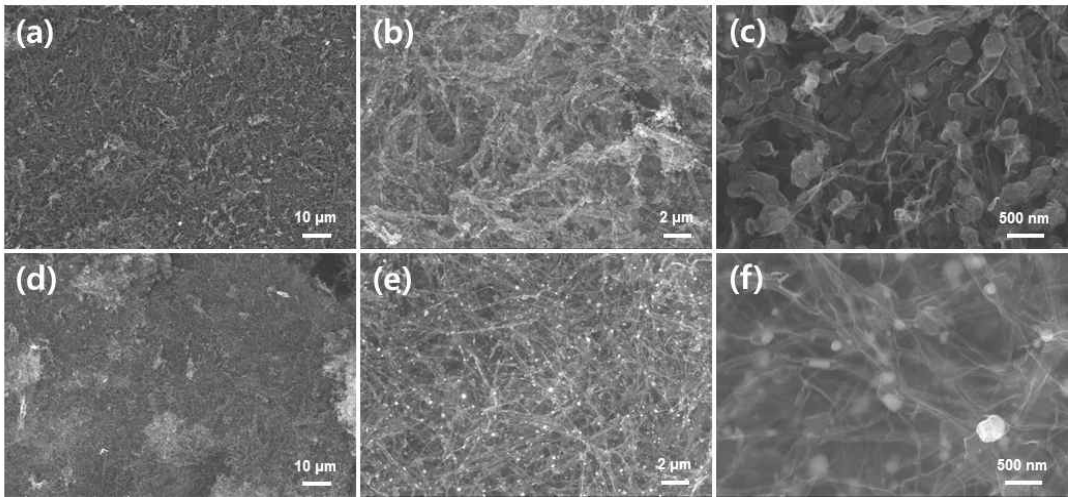

Figure 11. SEM images of bimetallic ZnCo ZIFs-derived monolithic fibers with a molar ratio of Zn:Co with (a-c) 3:7, (d-f) 0:10.

조선대학교
CHOSUN UNIVERSITY

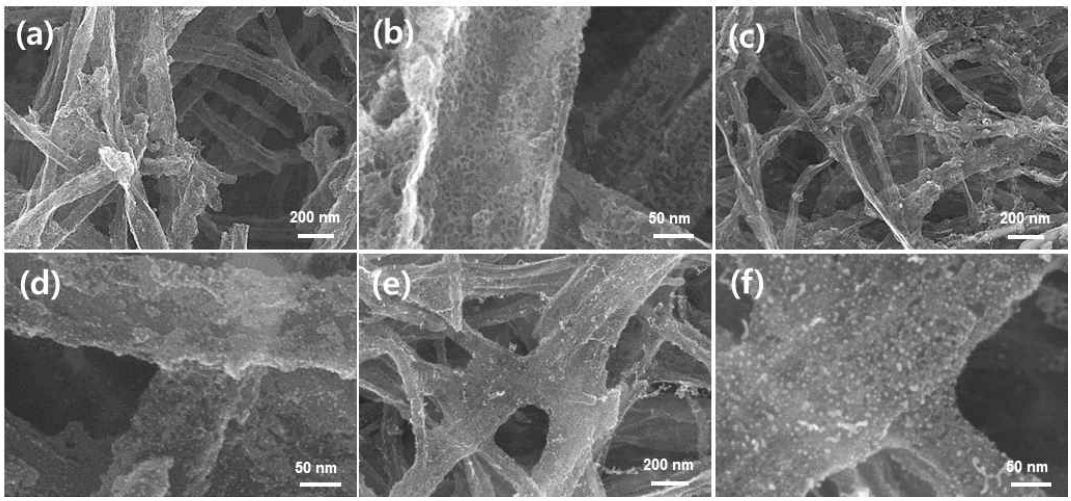

Figure 12. SEM images of (a,b) CoSA-N-C@Ru-0.1, (c,d) CoSA-N-C@Ru-0.5 and (e,f) CoSA-N-C@Ru-1.0.

조선대학교
CHOSUN UNIVERSITY

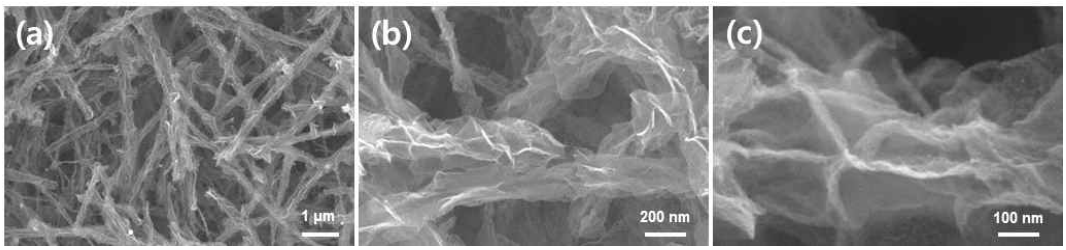

Figure 13. (a-c) SEM images of CoSA-N-C@Ru-5.0.

조선대학교
CHOSUN UNIVERSITY

The cross-section view SEM images in the Figure 8h confirmed that well-aligned carbon fibers were stacked without any cracks. Even though it was compressed by the pressure caused by vacuum filtration, the carbon fiber maintained the porous structure in the side-view as shown in Figure 8i-j. Also, the macropores generated in the tubular structure can be observed (white circles dotted in Figure 8j). In the high-resolution SEM of the carbon fibers in the middle of the membrane, a very small amount of Ru nanoparticles are observed, but it is much less than that in the fibers of the surface. Likewise, a similar phenomenon is observed in CoSA-N-C@Ru-1.0. Abundant Ru nanoparticles were observed in carbon fibers located on the surface of the membrane in Figure 14a-d, and relatively fewer Ru nanoparticles were observed in the inner part of the membrane in Figure 14e-h.

The uniform element distribution of the monolithic carbon network is shown by EDX elemental mapping of CoSA-N-C@Ru and CoSA-N-C@Ru-1.0 in Figure 15 and Figure 16. In CoSA-N-C@Ru, the C, Co, Ru and N elements were well distributed generally and in CoSA-N-C@Ru-1.0, the C, Ru and Co species were verified. In addition, as shown in Figure 8l of the cross-section of the CoSA-N-C@Ru membrane, Ru elements were most distributed on both surfaces of the monolithic carbon matrix and relatively little distribution on the inner-part, indicating that Ru was selectively deposited on the membrane surface. The similar phenomenon is observed in Figure 17 of the CoSA-N-C@Ru-1.0.

After the same amount of Ru deposition (0.25 ml), the morphology of N-C@Ru and CoNP-N-C@Ru was also observed as SEM in Figure 18. Ru nanoparticles were not observed in N-C@Ru, whereas it was uniformly distributed throughout in CoNP-N-C@Ru. It is explained that the presence of Co nanoparticles can control Ru deposition, and the interaction between Ru and Co has proven to further deposit Ru.

조선대학교
CHOSUN UNIVERSITY

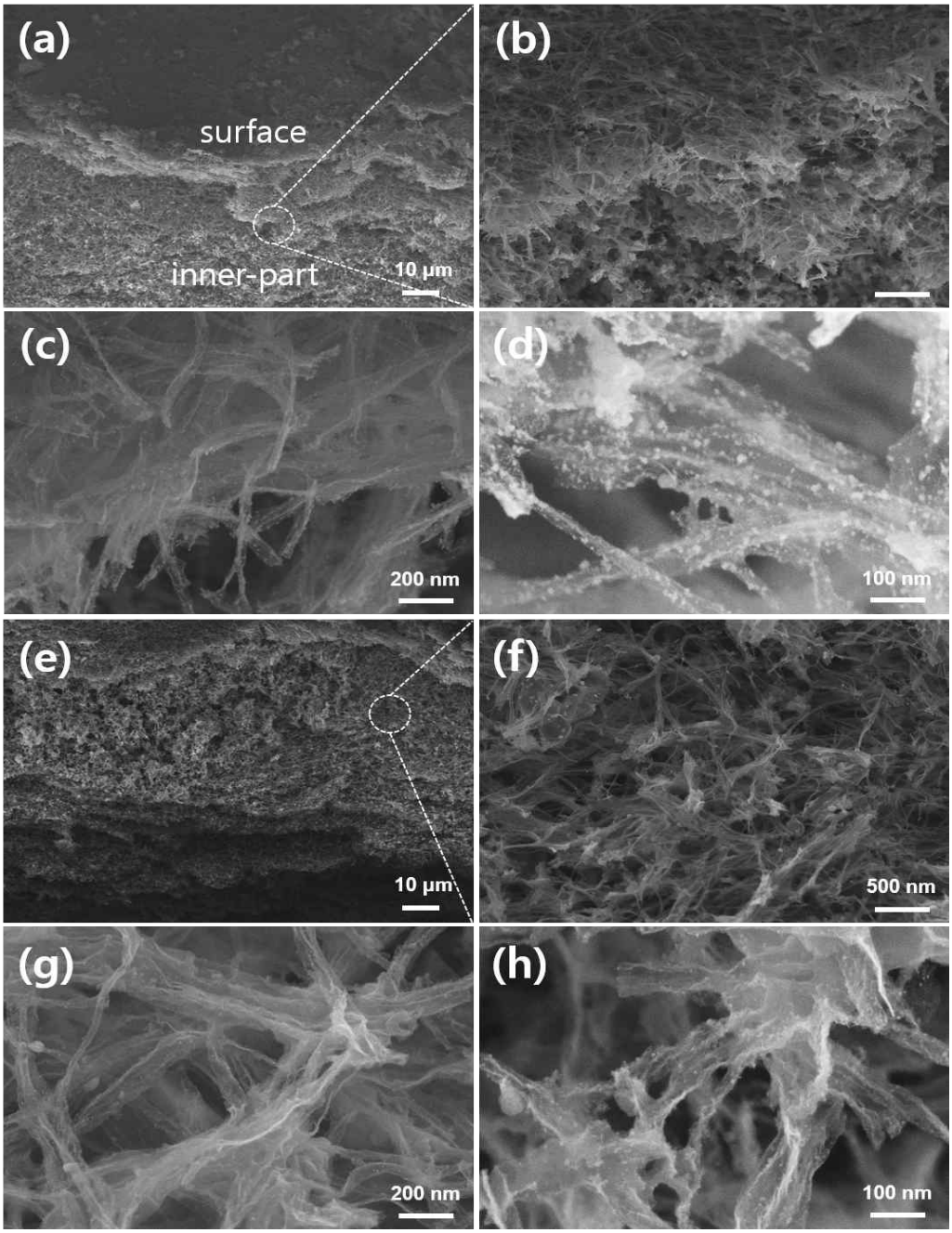

Figure 14. SEM images of CoSA-N-C@Ru-1.0. (a-d) Top-view SEM images at the surface of monolith, and (e-h) cross-sectional SEM images of the inner part of monolith.

조선대학교
CHOSUN UNIVERSITY

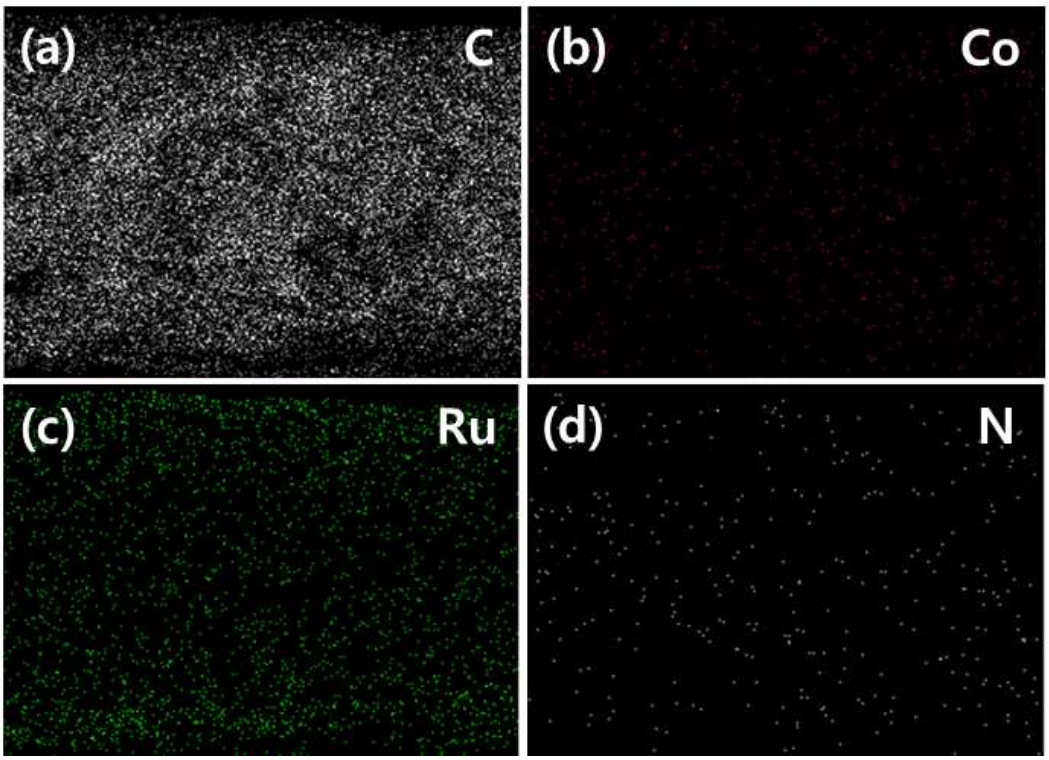

Figure 15. (a-d) Elemental mapping images of C, Co, Ru, N for CoSA-N-C@Ru.

조선대학교
CHOSUN UNIVERSITY

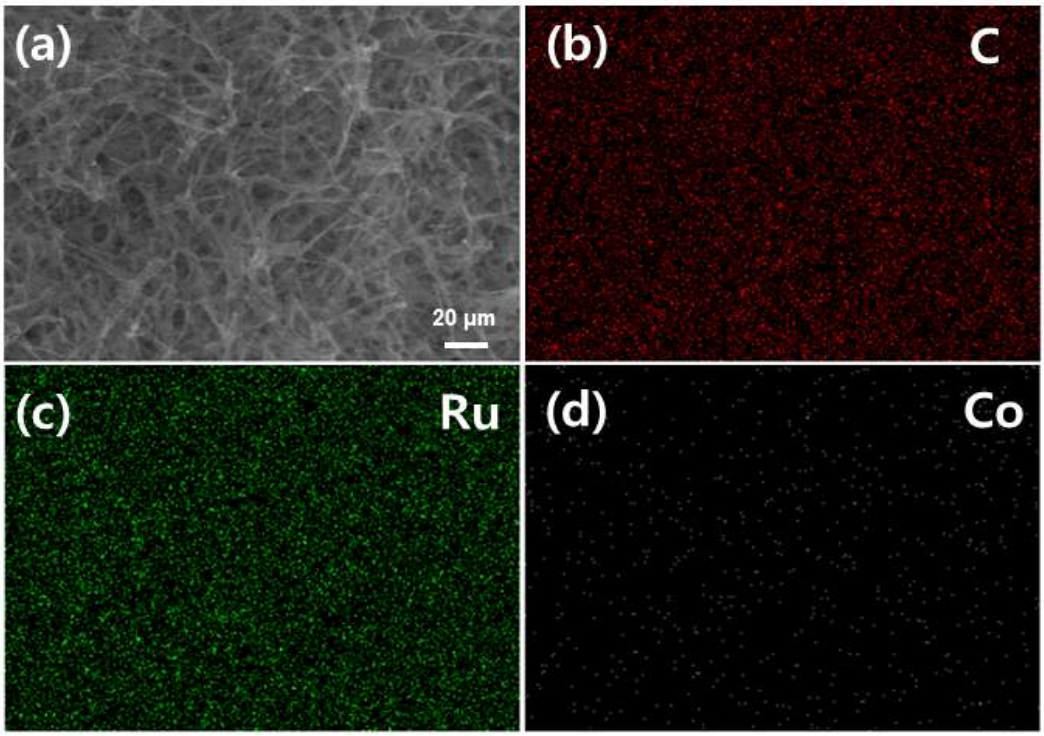

Figure 16. (a) SEM image and (b-d) elemental mapping images of C, Ru, Co for CoSA-N-C@Ru-1.0.

조선대학교
CHOSUN UNIVERSITY

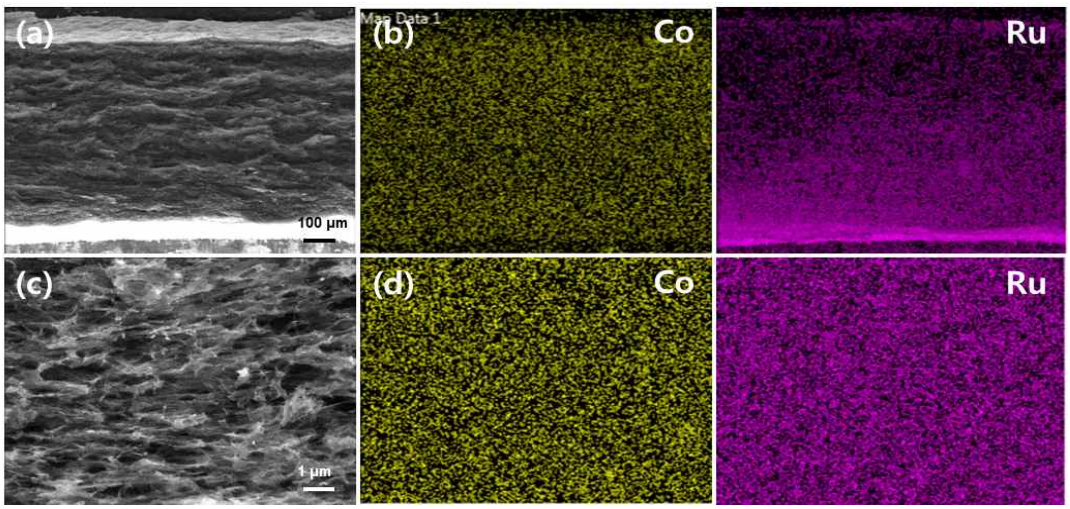

Figure 17. (a,c) Cross-sectional SEM images and (b,d) corresponding Co and Ru mapping images of CoSA-N-C@Ru-1.0.

조선대학교
CHOSUN UNIVERSITY

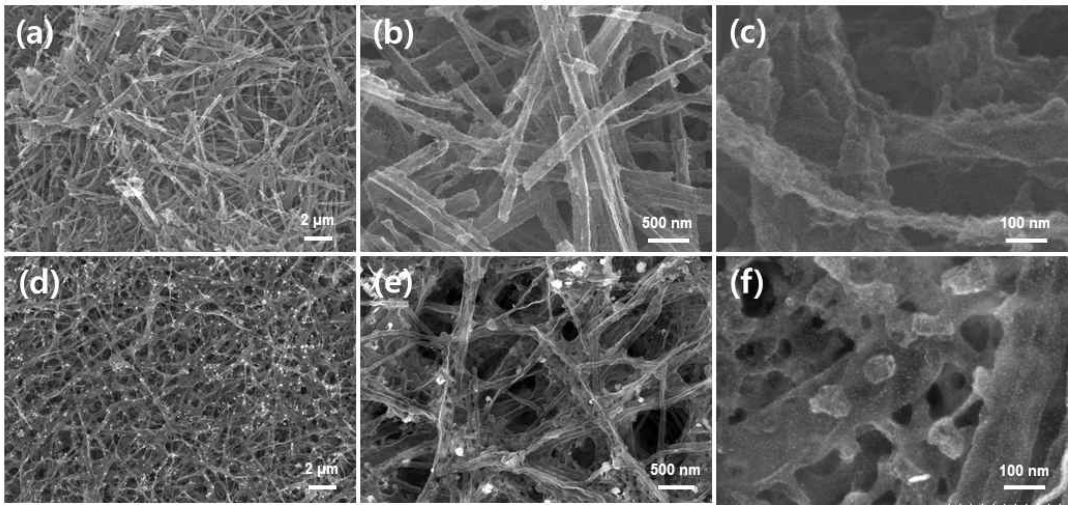

Figure 18. SEM images of (a-c) N-C@Ru and (d-f) CoNP-N-C@Ru.

조선대학교
CHOSUN UNIVERSITY

B. The crystallinity characterization of CoSA-N-C@Ru electrode

A more detailed structure of CoSA-N-C and CoSA-N-C@Ru was observed through transmission electron miroscope (TEM) and cs-corrected scanning transmission electron microscope (STEM). First of all, the porous structure of the surface is observed and no signals of metal particles are seen in TEM image in Figure 19a and STEM image in Figure 19b of the one-dimensional carbon nanofiber structure. In atomic-resolution high angle annular dark field STEM (HAADF-STEM) image (Figure 19c), the presence of single atomic Co is confirmed. In the STEM of CoSA-N-C@Ru, it can be observed that Ru particle is uniformly distributed throughout the nanofiber structure. In Figure 19e of STEM image, it was demonstrated that Co single atoms coexisted around Ru nanoparticles with an average size of 2-3 nm. As shown in the inset images of Figure 19e and 19f, the metal Ru have a lattice fringe of 0.214 nm corresponding to the (001) facet of metallic Ru [31]. Additionally, in Figure 19f and Figure 20 of CoSA-N-C@Ru it was showed the existence of Ru nanoparticles as well, and it was confirmed that the existence Ru nanoparticles and distribution of C, N, Co, Ru elements in the corresponding elemental mapping of Figure 20b. The overall distribution of Ru nanoparticles in CoSA-N-C@Ru-1.0 was also confirmed by TEM in Figure 21. The notable point is that the size of Ru nanoparticles is larger to ~15 nm. The elemental mapping of CoSA-N-C@Ru-1.0 is also shown in the Figure 22 and the C, N, Ru, and Co species are generally distributed entire of the structure.

The crystalline structure of the monolithic electrode was confirmed by X-ray diffraction (XRD) patterns. As shown in the Figure 23a, N-C and CoSA-N-C does not show any crystalline peak, which means that the carbon exists in the amorphous state and Co exists in an isolated single atomic state in carbon fibers. When Ru is deposited on CoSA-N-C, the weak peaks corresponding to metallic Ru is observed, which means some metallic Ru nanoparticles exist. The XRD patterns of bimetallic ZIF-derived nitrogen-doped carbon, which was controlled with the molar ratio of Zn and Co, were also investigated in Figure 23b. The results were consistent with those observed in the SEM, and as the molar ratio of Co to Zn increased, the peaks at 44° corresponding to (111) plane and at 51° corresponding to (002) plane also increased as the Co

조선대학교
CHOSUN UNIVERSITY

nanoparticles formed increasingly. Similarly, the XRD patterns for CoSA-N-C@Ru-X was also analyzed, indicating that the crystallinity of Ru also becomes stronger as the loading amount of Ru increases (Figure 23c).

조선대학교
CHOSUN UNIVERSITY

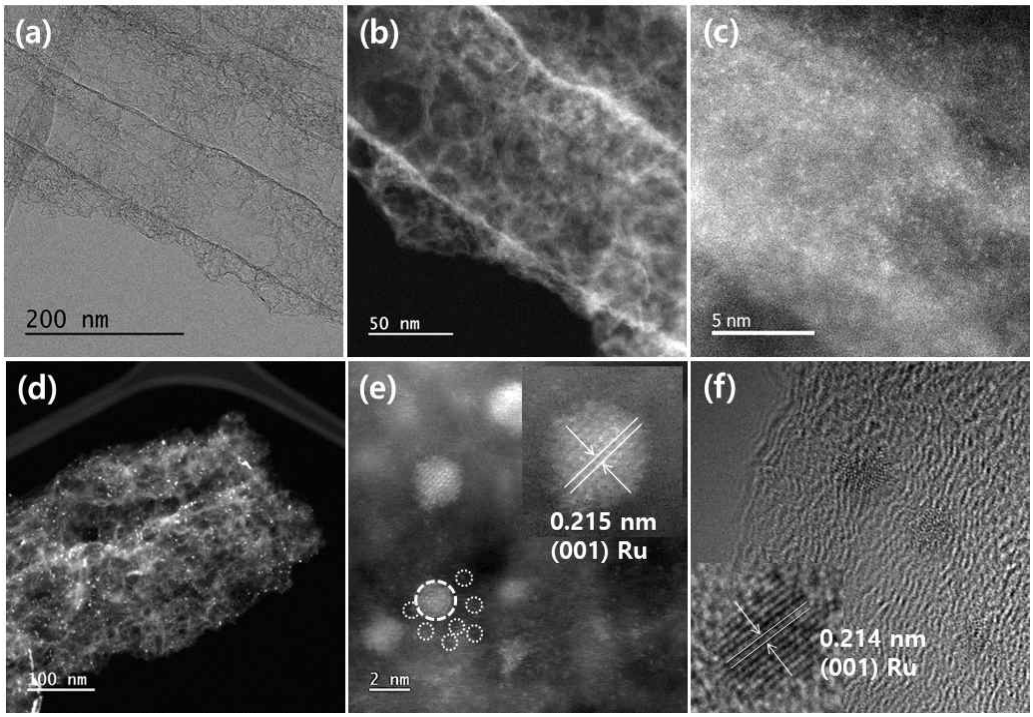

Figure 19. (a) TEM image, (b,c) STEM images of CoSA-N-C. (d) STEM image, (e) atomic-scale HAADF-STEM image and (f) TEM image of CoSA-N-C@Ru.

조선대학교
CHOSUN UNIVERSITY

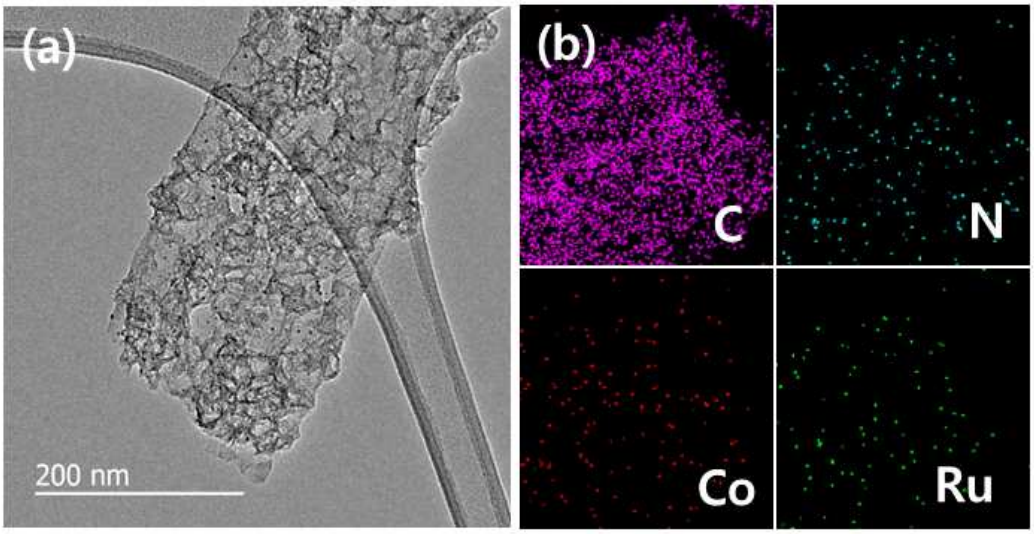

Figure 20. (a) TEM image of CoSA-N-C@Ru and (b) elemental mapping images of C, N, Co and Ru elements corresponding to Figure 19d.

조선대학교
CHOSUN UNIVERSITY

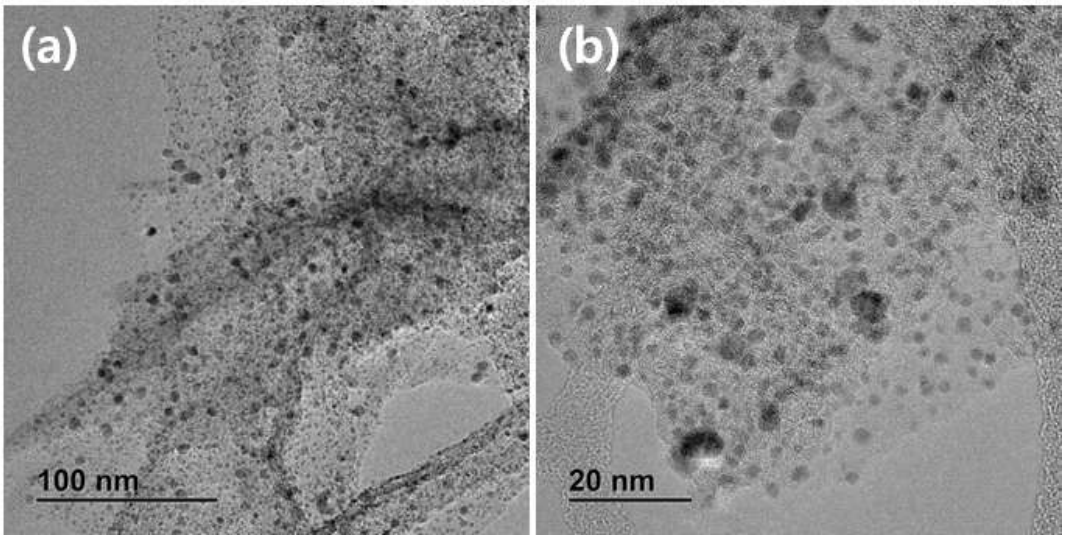

Figure 21. (a,b) TEM images of CoSA-N-C@Ru-1.0.

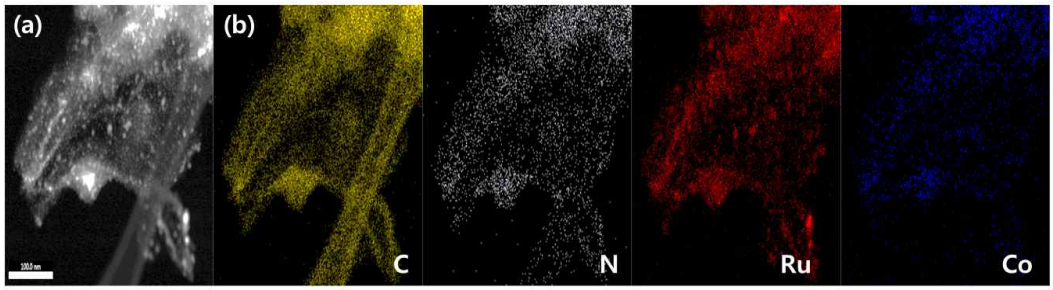

Figure 22. (a) STEM image of CoSA-N-C@Ru-1.0 and (b) corresponding elemental mapping images of C, N, Ru and Co.

조선대학교
CHOSUN UNIVERSITY

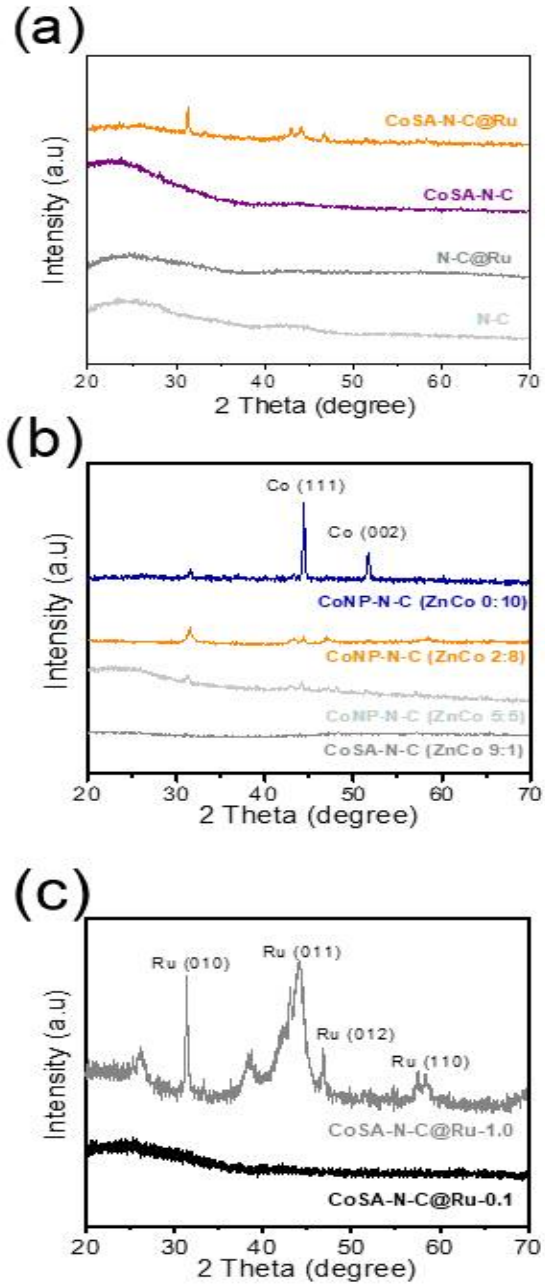

Figure 23. XRD patterns of (a) N-C, N-C@Ru, CoSA-N-C and CoSA-N-C@Ru, (b) bimetallic ZIF-derived carbon monoliths with a various molar ratio of Zn:Co. (c) CoSA-N-C@Ru-0.1 and CoSA-N-C@Ru-1.0.

조선대학교
CHOSUN UNIVERSITY

C. The characterization of CoSA-N-C@Ru to demonstrate of selective deposition of Ru

X-ray photoelectron spectroscopy (XPS) is performed to analyze the detailed structure of the monolith catalytic electrode. In the survey spectrum of Figure 24a, the presence of Ru, C, N, and Co of CoSA-N-C@Ru is confirmed well. In the Ru 3p spectrum, the two main peaks of 462.1 eV for Ru $3p_{3/2}$ and 484.4 eV for Ru $3p_{1/2}$ and two sub peaks of 466.0 eV for Ru $3p_{3/2}$ and 487.4 eV for Ru $3p_{1/2}$ assigned to metallic Ru and Ru-N bonding are shown in Figure 24b [32,33]. In N 1s spectrum of Figure 24c, N is deconvoluted to four peaks with pyrinidic, pyrrolic, graphitic, and oxidized N at 398.9 eV, 400.1 eV, 401.2 eV and 402.9 eV, respectively [34,35]. In the Ru 3d and C 1s spectrum of CoSA-N-C@Ru, Ru is deconvoluted with metallic Ru, Ru-N for Ru $3d_{5/2}$ at 280.4 eV, 281.1 eV and metallic Ru for Ru $3d_{3/2}$ at 284.7 eV [19,36,37], and C 1s is deconvoluted with C-C, C-N and C=O peaks at 284.9 eV, 286.3 eV and 288.2 eV, respectively (Figure 25b) [36,38]. In fine Co 2p spectrum of Figure 25c, any metallic Co peak does not appear, and Co^{3+}, Co^{2+} and nitrogen-coordinated Co with satellite peaks were observed in the surface XPS analysis of CoSA-N-C@Ru [39,40]. In depth profile spectrum of Ru 3p, as the etching time increases, the peak at 465.6 eV corresponding to Ru-N decreases and the peak of 461.3 eV corresponding to metallic Ru increases in Figure 24d. This result means that Ru is selectively deposited and embedded in the carbon framework to coordinate with nitrogen. In depth profile spectrum of Co 2p, the peak of surface corresponding to metallic Co was not manifested at first, but it is observed that a distinct peak appears as the etching time increases (Figure 24e). It means that the embedded Co appears as the carbon layer is etched. This phenomenon is similar in Ru 3d, where C-N peak and Ru-N peak become weaker in the Ru 3d spectrum overlapping C 1s in Figure 25a. To compare the differences in Ru 3p spectrum in the case of absence of Co and effect of different amount of Ru, fine Ru 3p spectrums of N-C@Ru, CoSA-N-C@Ru-0.1, CoSA-N-C@Ru and CoSA-N-C@Ru-1.0 is shown in Figure 24f. As the result, the peaks of Ru 3p for N-C@Ru loacated at 462.6 eV and 484.8 eV were shifted to lower binding energy of ~ 0.5 eV for CoSA-N-C@Ru by the incorporation of Co single atoms and

조선대학교
CHOSUN UNIVERSITY

nanoparticles, which is reported to stimulate the electron structure of Ru [41]. In Figure 26a, the notable point is as the amount of Ru decreases, Ru-N content increases and Ru content decreases. In the Figure 27a, the presence of C, N, and Co of CoSA-N-C is clearly confirmed, and in the C 1s spectrum of the Figure 27b, five peaks of C=C, C-C, C-N, C-O, and C=O were deconvolved at 284.5 eV, 285.1 eV, 286.2 eV, 287.6 eV and 289.9 eV, respectively [42,43]. And in the N 1s spectrum, there was no significant difference from CoSA-N-C@Ru (Figure 27c). Fine Ru 3d and N 1s spectra of N-C@Ru, CoSA-N-C@Ru-0.1 and CoSA-N-C@Ru-1.0 had similar relative intensity and peak position (Figure 28 and Figure 29).

조선대학교
CHOSUN UNIVERSITY

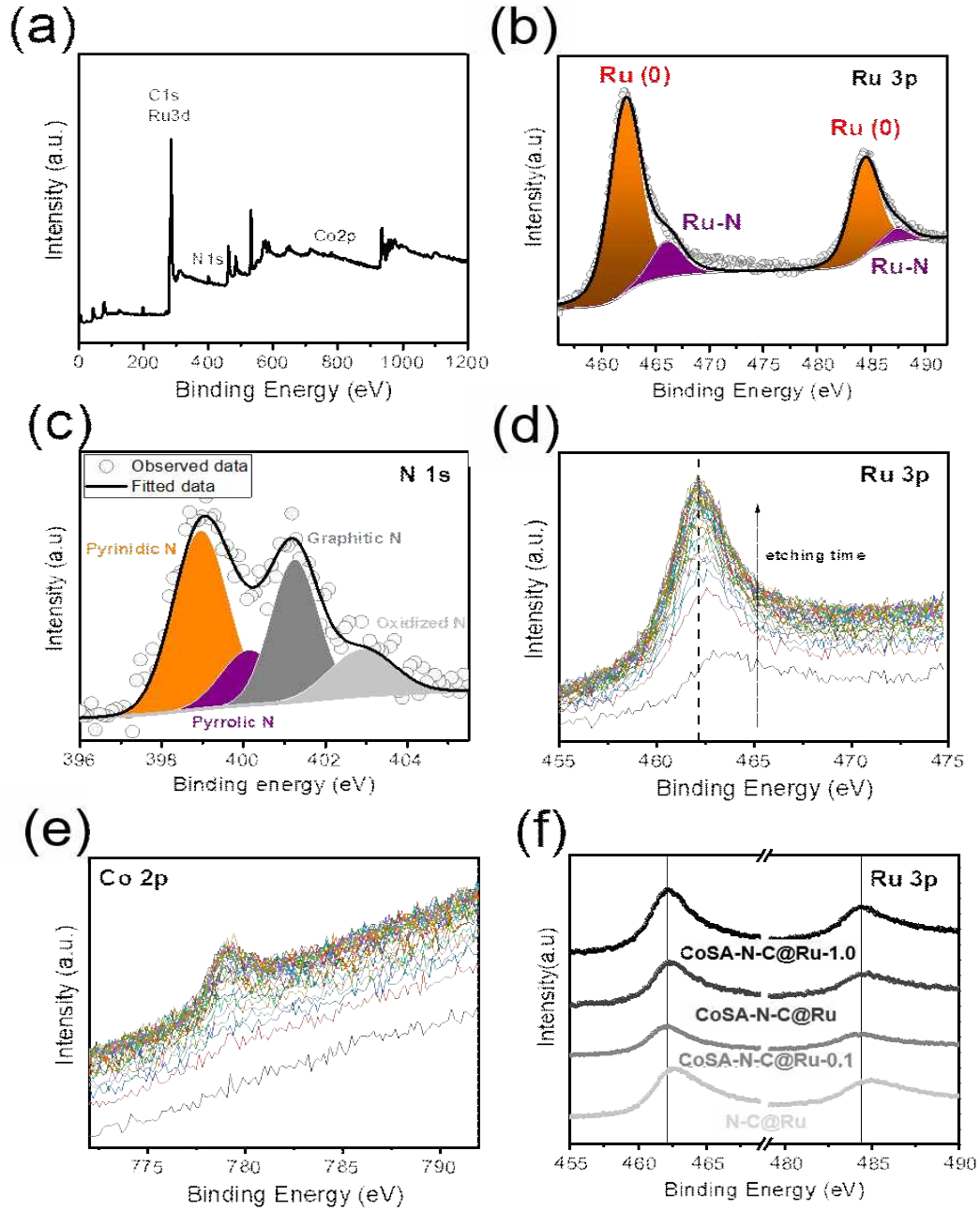

Figure 24. (a) XPS survey spectrum, and fine (b) Ru 3p, (c) N 1s spectrums of CoSA-N-C@Ru. Depth profile of CoSA-N-C@Ru for XPS fine (d) Ru 3p, (e) Co 2p spectrums. (f) The comparison of Ru 3p spectrums of N-C@Ru, CoSA-N-C@Ru-0.1, CoSA-N-C@Ru and CoSA-N-C@Ru-1.0.

조선대학교
CHOSUN UNIVERSITY

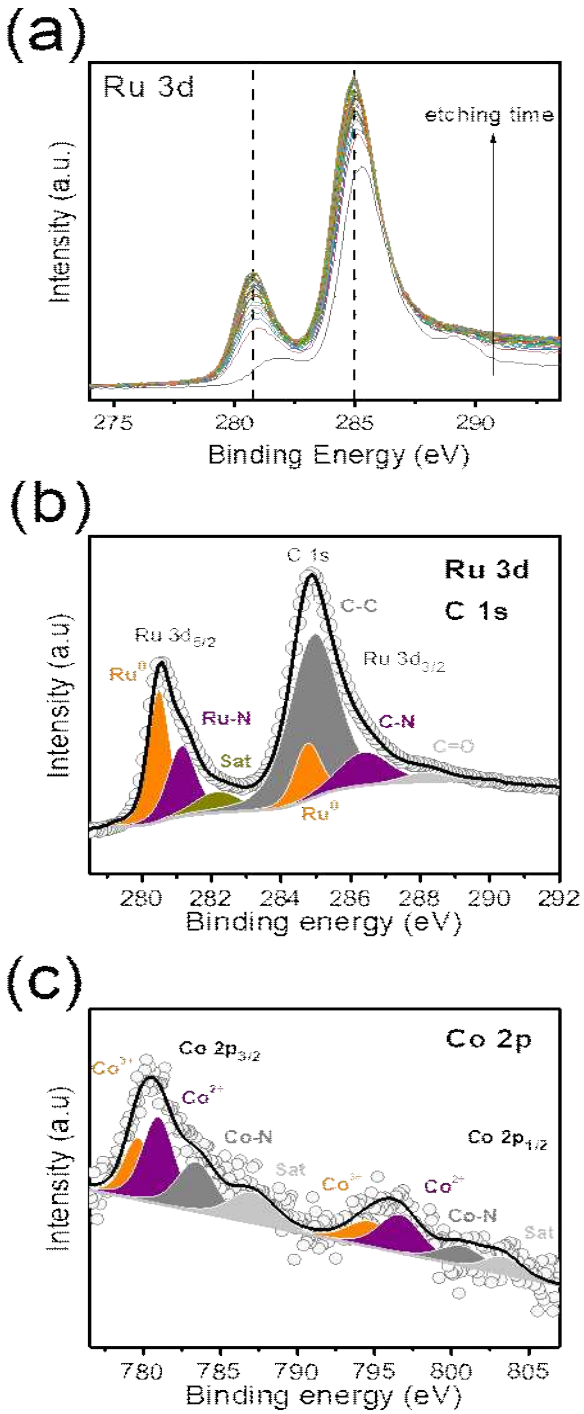

Figure 25. (a) Depth-profile of CoSA-N-C@Ru in Ru 3d spectrum. Fine (b) Ru 3d, (c) Co 2p spectrums of CoSA-N-C@Ru.

조선대학교
CHOSUN UNIVERSITY

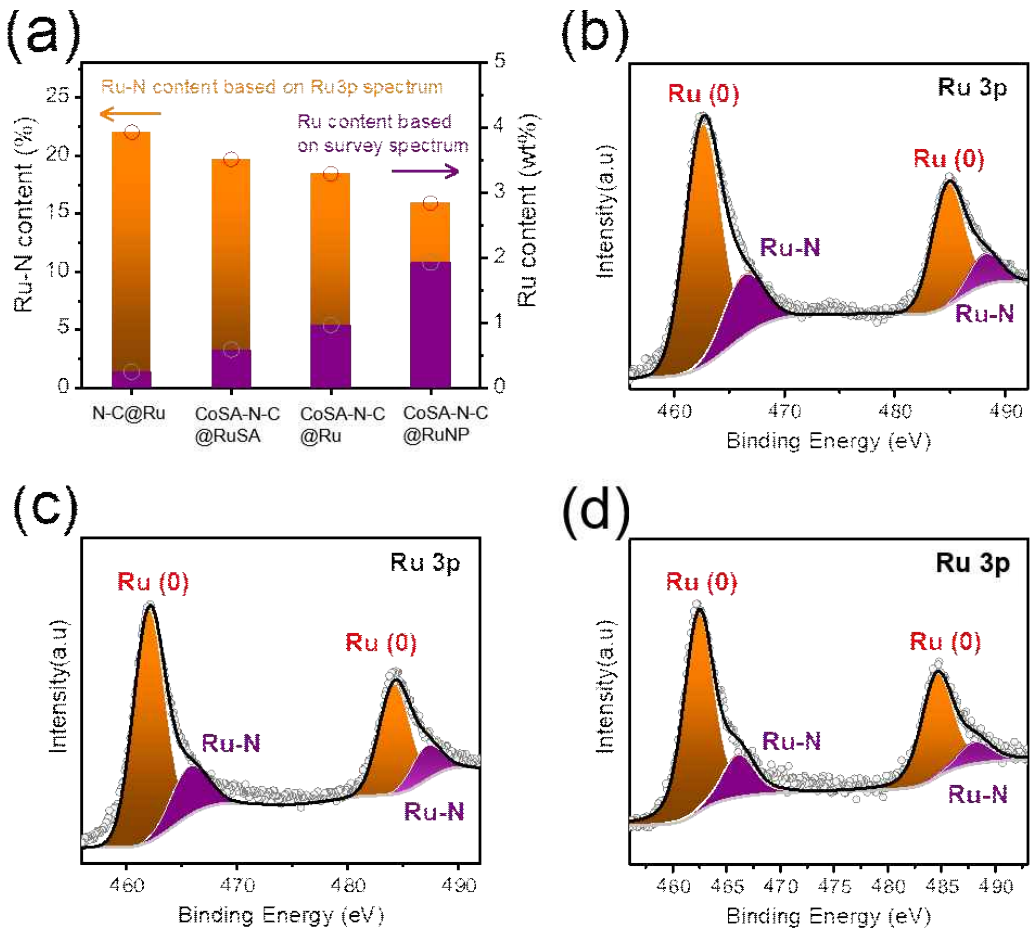

Figure 26. (a) The comparison of Ru-N and Ru content of N-C@Ru, CoSA-N-C@Ru-0.1, CoSA-N-C@Ru and CoSA-N-C@Ru-1.0. Fine Ru 3p spectrums of (b) N-C@Ru, (c) CoSA-N-C@Ru-0.1, (d) CoSA-N-C@Ru-1.0.

조선대학교
CHOSUN UNIVERSITY

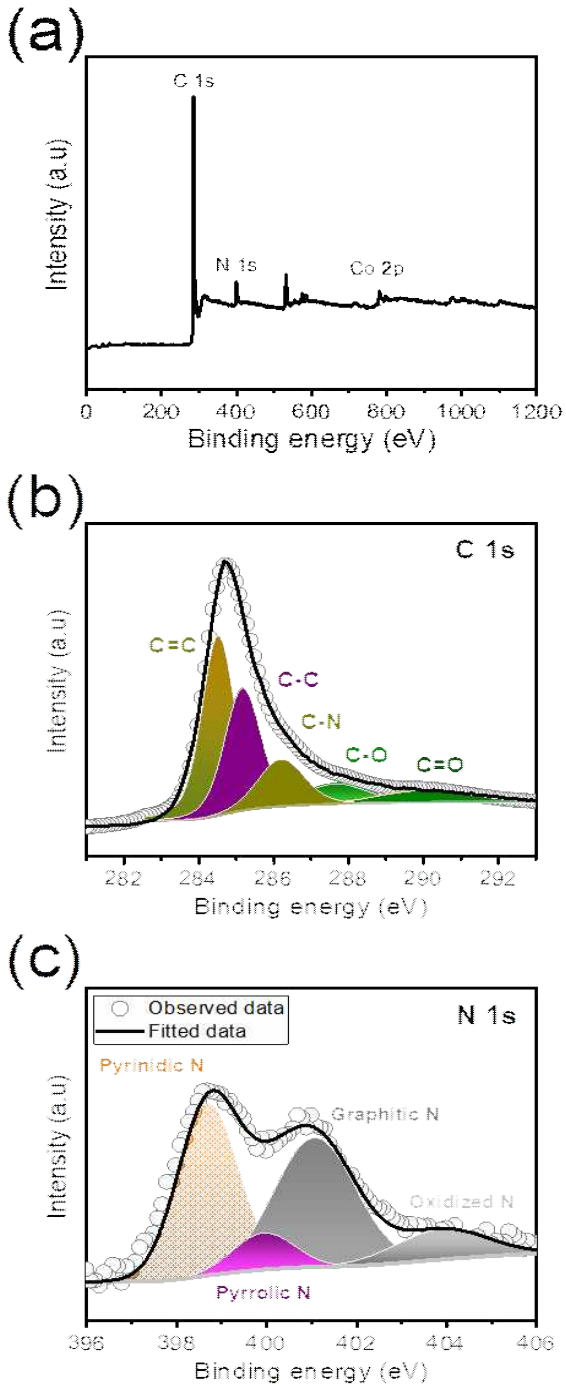

Figure 27. (a) XPS survey spectrum, and fine XPS (b) C 1s, (c) N 1s spectrums of CoSA-N-C.

조선대학교
CHOSUN UNIVERSITY

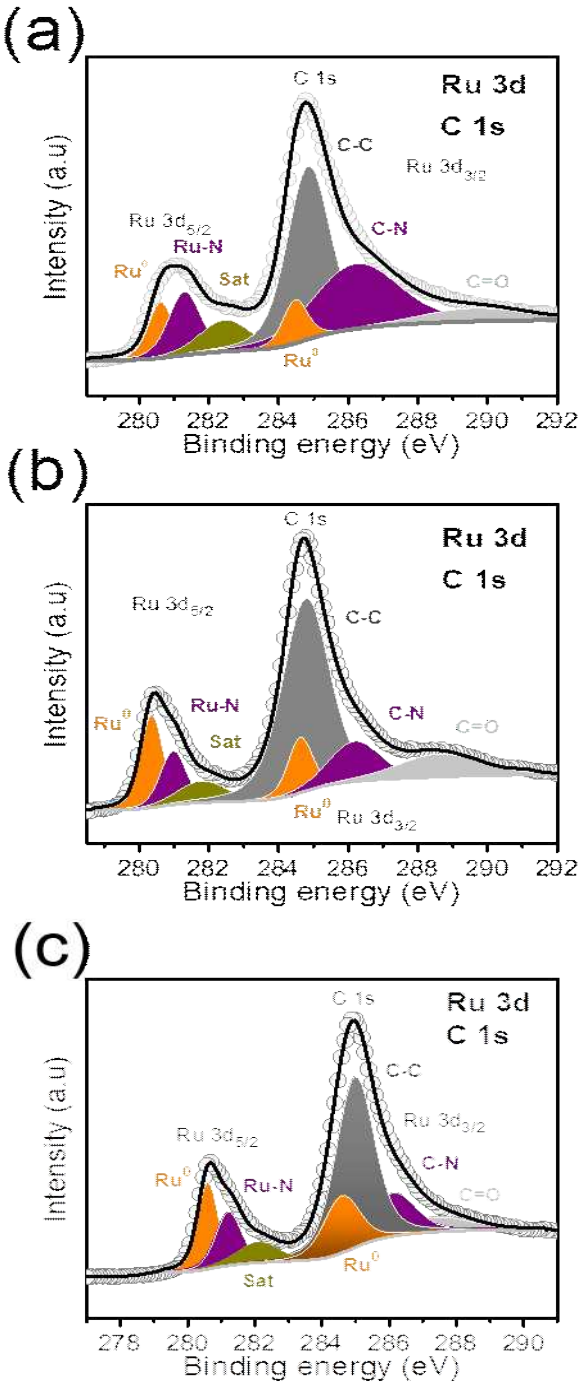

Figure 28. Fine Ru 3d spectrums of (a) N-C@Ru, (b) CoSA-N-C@Ru-0.1, (c) CoSA-N-C@Ru-1.0.

조선대학교
CHOSUN UNIVERSITY

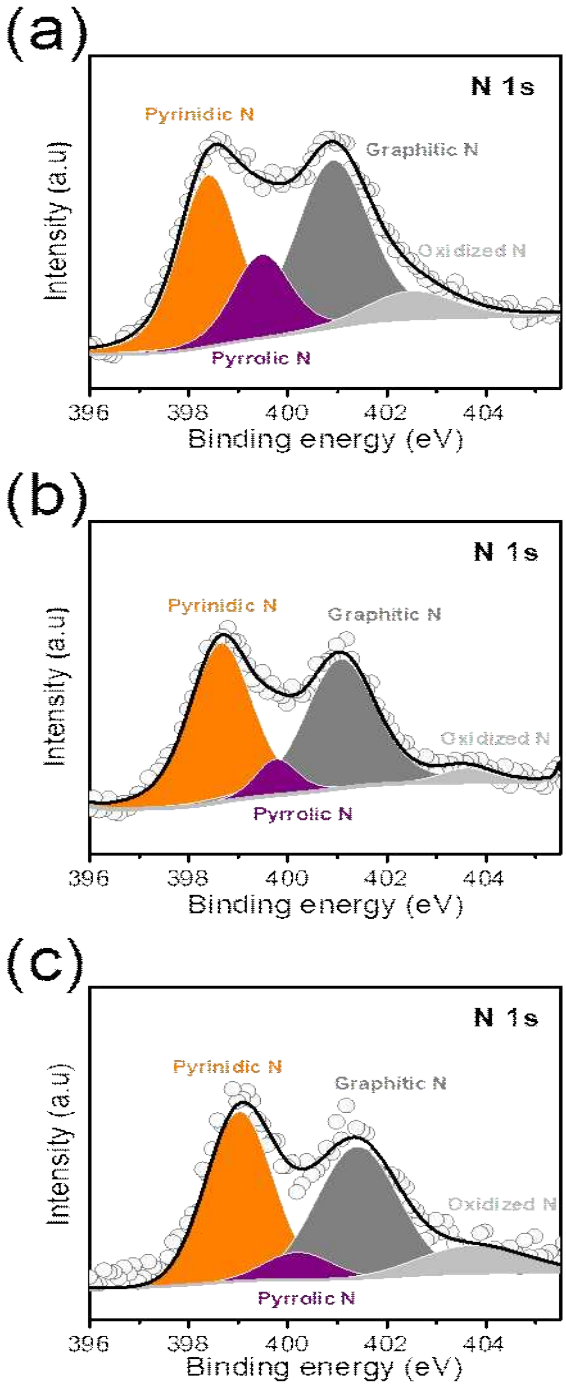

Figure 29. Fine N 1s spectrums of (a) N-C@Ru, (b) CoSA-N-C@Ru-0.1, (c) CoSA-N-C@Ru-1.0.

조선대학교
CHOSUN UNIVERSITY

To measure the metal contents, inductively coupled plasma-mass spectrometry (ICP-MS) and thermogravimetric analysis (TGA) were performed. In Table 1, the Ru content of CoSA-N-C@Ru and CoSA-N-C@Ru-1.0 was revealed to be about 0.32 wt% and 2.58 wt%, respectively. The total metal content of CoSA-N-C@Ru through TGA analysis was less than 1.5 wt%. It should be noted that the Ru content on the surface of the monolithic carbon membrane through XPS and EDS is relatively high compared to the results obtained by ICP-MS and TGA. This result means that Ru is selectively deposited on the carbon surface and more Ru is on the surface.

The Figure 30 shows N_2 adsorption-desorption isotherm curves, and specific surface areas of CoSA-N-C and CoSA-N-C@Ru which is calculated based on the Brunauer-Emmett-Teller (BET) method. The average pore size of CoSA-N-C was 9.96 nm and a specific surface area was 996 m^2g^{-1}, and the average pore size of CoSA-N-C@Ru reduce slightly to 8.80 nm and the specific surface area to 986 m^2g^{-1} while Ru was deposited in the pores of the carbon monolith surface. As shown in the Figure 30b, the pore size distribution of CoSA-N-C represents two main peaks, the front narrow peak corresponding to nanopores and the wide peak corresponding to meso/macropores. The intensity of the nanopores slightly reduces and the pore distribution of meso/macrpore is narrowed by the deposition on surface of CoSA-N-C@Ru. This result means that Ru nanoparticles deposit onto nanopores generated by ZIF and meso/macropores generated by tubular fibrous structure in the carbon matrix.

조선대학교
CHOSUN UNIVERSITY

Sample	Metal	XPS (wt%)	EDS (wt%)	TGA (wt%)	ICP-MS (wt%)
NC@Ru	Ru	0.25	-	-	-
CoSA-NC@Ru	Co	1.01	1.37	Co+Ru ~1.5wt%	1.21
	Ru	0.97	1.44		0.32
CoSA-NC@Ru-0.1	Co	0.99	-	-	-
	Ru	0.59			
CoSA-NC@Ru-1.0	Co	1.12	3	Co+Ru ~4.0wt%	1.14
	Ru	1.93	23		2.58

Table 1. Metal loading of N-C@Ru, CoSA-N-C@Ru, CoSA-N-C@Ru-0.1 and CoSA-N-C@Ru-1.0 measured from XPS, EDS, TGA and ICP-MS.

조선대학교
CHOSUN UNIVERSITY

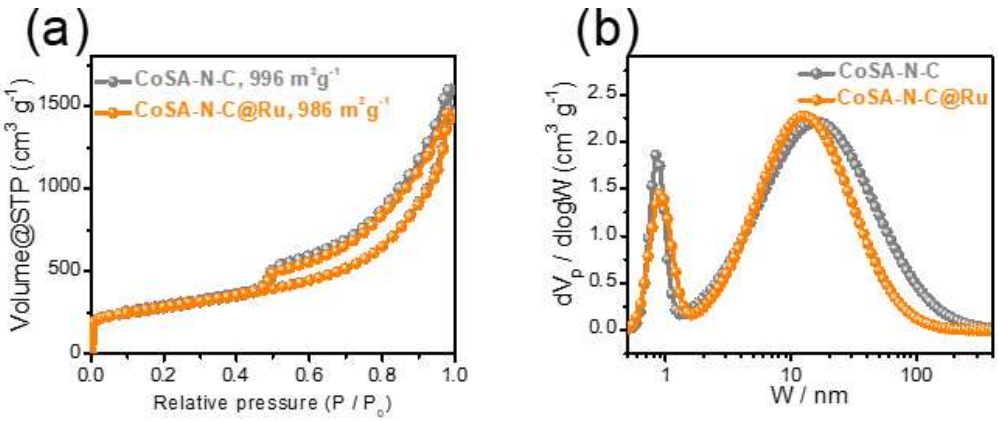

Figure 30. (a) N_2 adsorption-desorption isotherm curves, (b) pore size distribution of CoSA-N-C and CoSA-N-C@Ru.

조선대학교
CHOSUN UNIVERSITY

D. The pH-universal activity toward Hydrogen Evolution Reaction of CoSA-N-C@Ru catalytic electrode

The HER activity of N-C@Ru, CoSA-N-C, CoSA-N-C@Ru and Pt/C was measured with a three-electrode configuration in 1 M KOH, as an alkaline electrolyte. In the LSV curves shown in the Figure 31a, N-C@Ru and CoSA-N-C showed poor activity, requiring high overpotential values of 73 mV and 152 mV to achieve a current density of 10 mA cm^{-2}, respectively. In contrast, CoSA-N-C@Ru achieved 10 mA cm^{-2} with only 14 mV of overpotential, which was much smaller than the value of Pt/C (24 mV), indicating excellent HER performance in the alkaline electrolyte. In addition, to achieve a current density of 100 mA cm^{-2}, CoSA-N-C@Ru requires the smallest overpotential of 137 mV and is much smaller than the value of Pt/C (278 mV). As shown in Figure 31b, the CoSA-N-C@Ru has a value of 19 mV dec^{-1} of tafel slope which is much smaller than that of Pt/C (32 mV dec^{-1}), meaning that CoSA-N-C@Ru produces hydrogen through the Volmer-Tafel mechanism [44]. In addition, in the nyquist plot of Figure 32a, the smallest charge-transfer resistance (R_{ct}) of CoSA-N-C@Ru was observed to explain efficient HER performance in alkaline electrolyte.

Next, SCN^- ion and EDTA (ethylenediaminetetraacetic acid) were introduced to figure out the roles of active sites. SCN^- ion as known to block active sites was first introduced to determine the contribution of HER activity of single atomic Co and nanoparticles Ru in alkaline electrolyte. With the introduction of SCN^- ion, the HER performance of CoSA-N-C@Ru became worse rapidly, which means the Ru nanoparticles located at the surface of monolith work as a active site that directly affects HER performance (Figure 31c). When EDTA is introduced in alkaline electrolyte, the HER activity of CoSA-N-C@Ru is lower than original activity. And a similar tendency was shown in nyquist plots (Figure 32b).

Also, HER activity was measured with a three-electrode configuration in 0.5 M H_2SO_4, as an acidic electrolyte. In Figure 33a, CoSA-N-C@Ru shows a very small $\eta_{j=10}$ value of 11 mV, slightly larger than that of Pt/C (7 mV), and much smaller than N-C@Ru (214 mV), CoSA-N-C(273 mV). To achieve 100 mA cm^{-2}, CoSA-N-C@Ru

조선대학교
CHOSUN UNIVERSITY

also required only 152 mV of overpotential, slightly larger than of Pt/C (141 mV) and much smaller than that of other control samples CoSA-N-C (314 mV) and N-C@Ru (228 mV). The resulting tafel plot showed similar tendency, CoSA-N-C@Ru showing a low slope value of 21.3 mV dec^{-1}, similar to Pt/C (15.5 mV dec^{-1}), and much lower than the slope of other control samples (88 mV dec^{-1} for N-C@Ru and 136 mV dec^{-1} for CoSA-N-C) in Figure 33b. In both alkaline and acidic electrolyte measured HER activity shows the best results among recently reported Ru-based catalysts considering the overpotential to achieve a current density of 10 mA cm^{-2} and tafel slopes required [19-22,45-50]. Similarly, the nyquist plot in the Figure 34a shows the smaller charge-transfer resistance (R_{ct}) than Pt/C to explain efficient HER performance in acidic electrolyte, too. The noteworthy point is that the HER activity of CoSA-N-C@Ru in alkaline and acidic electrolytes is the most excellent among the latest reported Ru based electrocatalysts in terms of the overpotential to achieve 10 mA cm^{-2} of current density and the tafel slopes with ultralow Ru loading, as summarized in Table 2.

Similarly, in order to know the contribution of active sites under acidic conditions, SCN^- ion and EDTA were additionally introduced to measure HER activity. As shown in Figure 33c, when SCN^- ion and EDTA were introduced, HER performance showed a similar trend to the results in the alkaline electrolyte. When the EDTA was added, the HER performance decreased considerably, and the HER activity decreased rapidly when SCN^- was added. The similar tendency was observed in nyquist plots of Figure 34b.

HER performances of CoNP-N-C and N-C were additionally analyzed in both alkaline and acidic conditions to determine the contribution of Co nanoparticles to HER activity. All of these Ru-free catalyst showed poor HER activity in alkaline and acidic condition (Figure 35 a,b). In addition, to confirm the change in HER performance according to the reacting amount of Ru, the HER performance of CoSA-N-C@Ru-X (X is 0.1, 0.5, 1.0 and 2.0 in this part) were further measured in both alkaline and acidic electrolytes (Figure 35c, d). As a result, it was found that the performance did not improve significantly as the amount of reacting amount of Ru increased. Thus, it is noteworthy that when Co exists in the single atomic state, it exhibits the most efficient synergistic effect when reacted with an appropriate amount of Ru.

조선대학교
CHOSUN UNIVERSITY

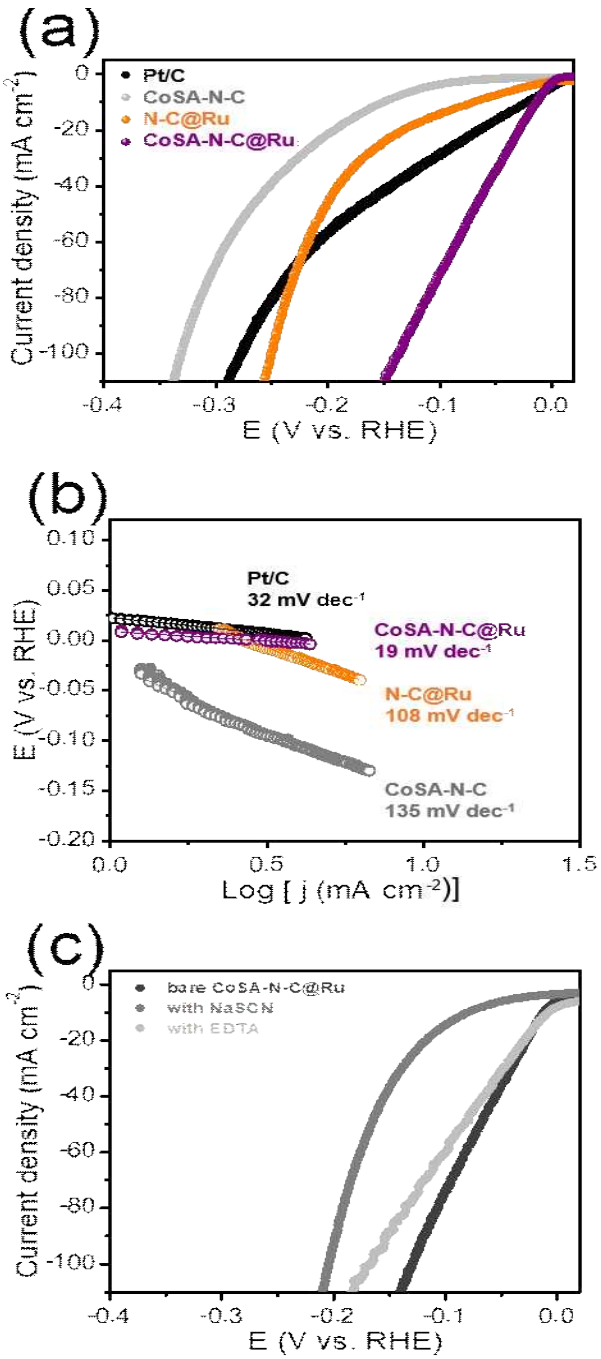

Figure 31. (a) LSV curves, (b) corresponding Tafel plots in alkaline electrolyte (1 M KOH) with a scan rate of 0.1 mV s^{-1}. (c) LSV curves of CoSA-N-C@Ru in 1 M KOH electrolyte with NaSCN and EDTA.

조선대학교
CHOSUN UNIVERSITY

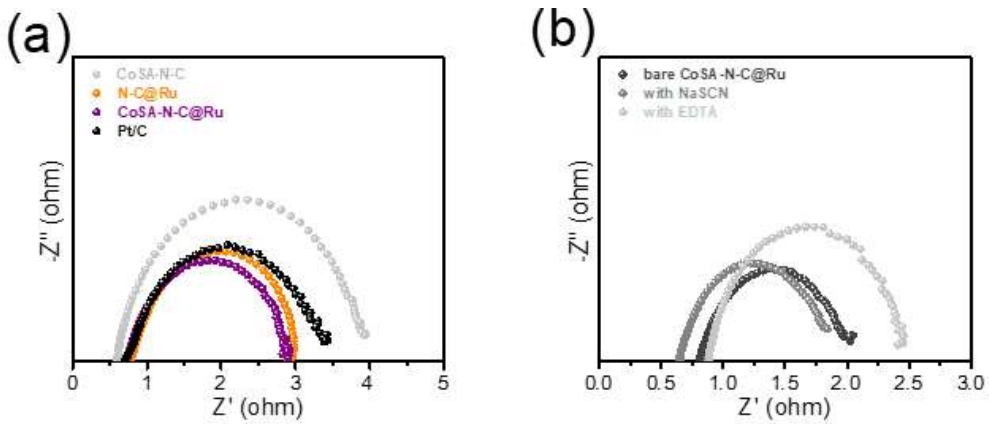

Figure 32. (a,b) Nyquist plots in an alkaline electrolyte.

조선대학교
CHOSUN UNIVERSITY

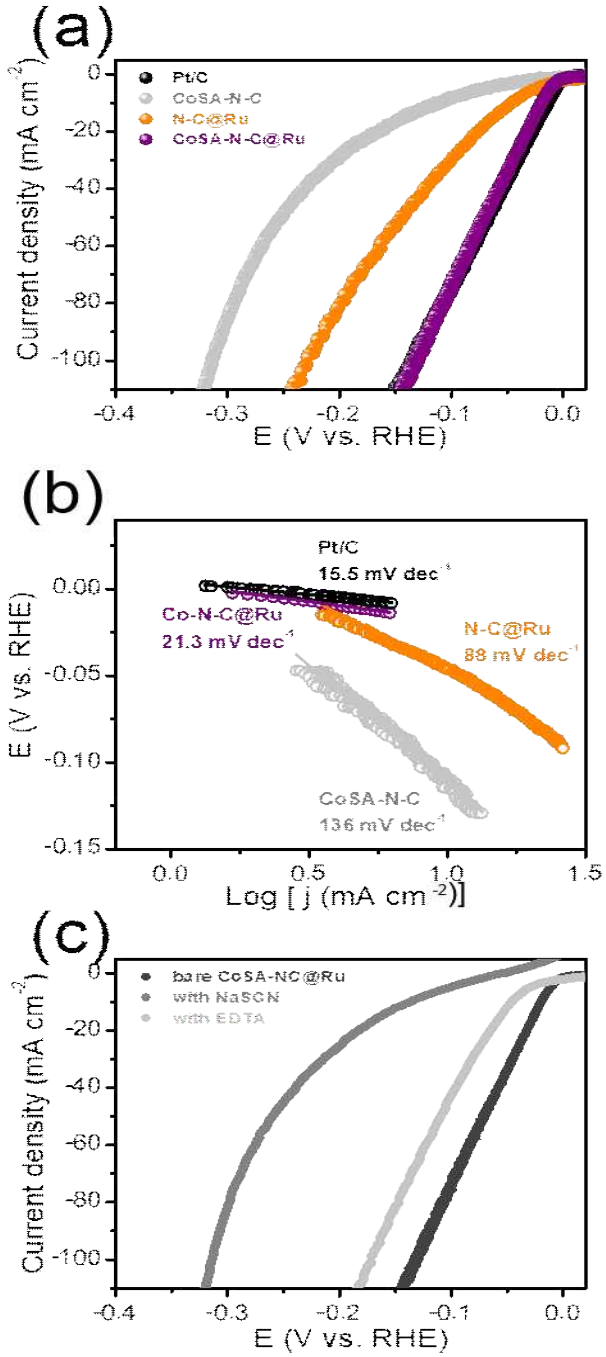

Figure 33. (a) LSV curves, (b) corresponding Tafel plots in acidic electrolyte (0.5 M H_2SO_4) with a scan rate of 0.1 mV s^{-1}. (c) LSV curves of CoSA-N-C@Ru in 0.5 M H_2SO_4 electrolyte with NaSCN and EDTA.

조선대학교
CHOSUN UNIVERSITY

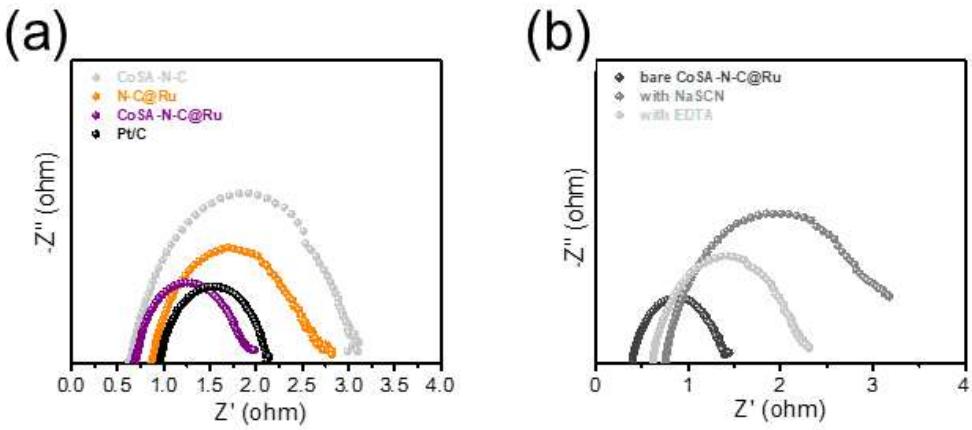

Figure 34. (a,b) Nyquist plots in an acidic electrolyte.

조선대학교
CHOSUN UNIVERSITY

Catalyst	Substrate	Electrolytes	η at j (mV@ mA cm^{-2})	Tafel plot (mV dec^{-1})	Catalyst loading ($mgcm^{-2}$)	Ru loading (wt%)	Ru loading (μgcm^{-2})	references
CoSA-NC@Ru	freestanding	1 M KOH	14@10	19	7.3	0.32	23.4	this work
		0.5 M H_2SO_4	15@10	17				
[Ru(SA)–Ru(NP)/@ RuNx@GN]/GN	glassy carbon	1 M KOH	7@10	20	0.284	16	45.4	Adv. Energy Mater. 9 (2019), 1900931
		0.5 M H_2SO_4	10@10	28	0.354			
RuCoP	glassy carbon	0.5 M H_2SO_4	11@10	37	0.3	40	120	Energy Environ. Sci., 11 (2018), 1819--1827
		1M KOH	23@10	31				
Ru@Co-SAs /N-C	glassy carbon	1 M KOH	7@10	30	0.285	5.36	15.3	Nano Energy 59 (2019) 472-480
		0.5 M H_2SO_4	57@10	55				
RuP_2@NPC	glassy carbon	1 M KOH	52@10	69	1	-	-	Angew. Chem. Int. Ed. 56 (2017) 11559
		0.5 M H_2SO_4	38@10	38				
Ru@C_2N	glassy carbon	1 M KOH	17@10	38	0.285	28.7	81.80	Nat. Nanotechnol. 12 (2017) 441
		0.5 M H_2SO_4	22@10	30				
Ru/C_3N_4/C	glassy carbon	0.1 M KOH	79@10	-	0.204	-	-	J. Am. Chem. Soc. 138 (2016) 16174
		0.5 M H2SO4	~75@10	-				
Ru@CN-0.16	glassy carbon	1 M KOH	32@10	53	0.246	3.18	7.8	Energ. Environ. Sci. 11 (2018) 800
		0.5 M H_2SO_4	126@10	-				
RuCo alloy/carbon	glassy carbon	1 M KOH	28@10	31	0.275	-	-	Nat. Commun. 8 (2017) 14969
Ru/Fe-N-C	glassy carbon	1M KOH	9@10	28	0.485	4.92	23.9	Adv. Sci. 8 (2021), 2001881
Ru-MnFeP/NF	nickel foam	1M KOH	35@10	36	-	1.08	-	Adv. Energy Mater. 10 (2020), 2000814
Ru-MoS2/CC	carbon cloth	1 M KOH	41@10 171@100	114	12.4	0.37	46	Appl. Catal. B 249 (2019) 91–97
		0.5 M H_2SO_4	61@10	-				

Table 2. Comparison of electrochemical activity of CoSA-N-C@Ru and recently reported Ru-based electrocatalysts toward HER.

조선대학교
CHOSUN UNIVERSITY

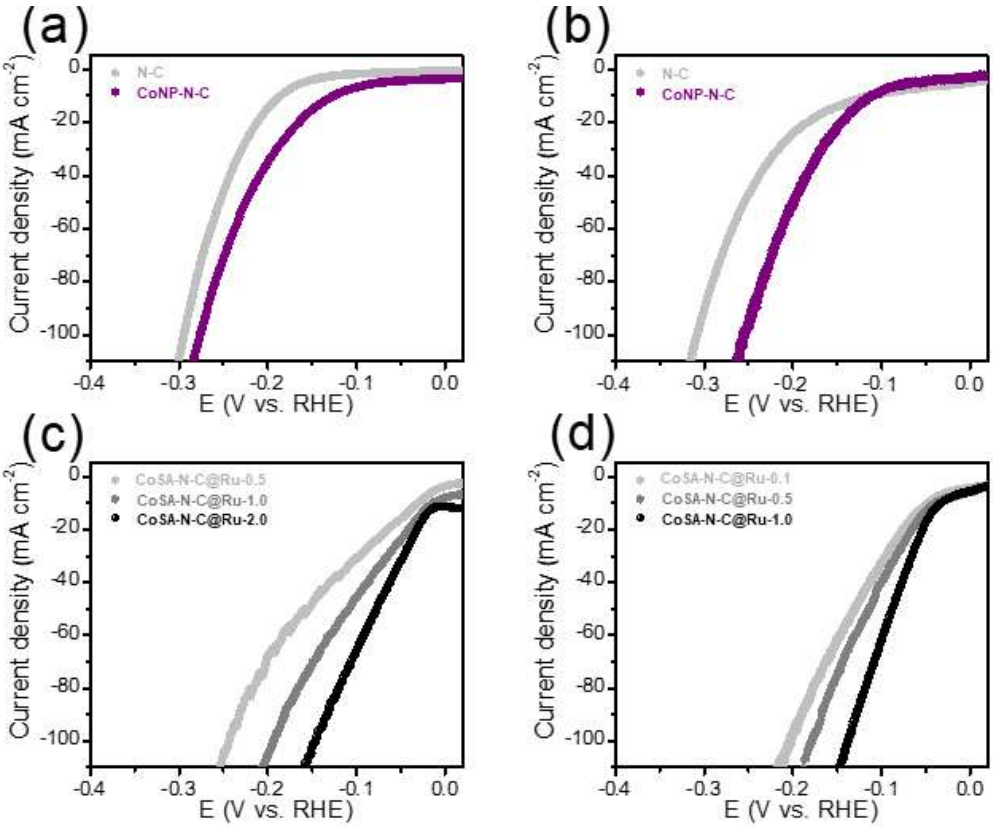

Figure 35. (a) LSV curves of N-C and CoNP-N-C (a) in an alkaline condition, (b) in an acidic condition. LSV curves of CoSA-N-C@Ru-X (c) in an alkaline condition, (d) in an acidic condition.

조선대학교
CHOSUN UNIVERSITY

E. The durability of CoSA-N-C@Ru electrode and overall water splitting with CoSA-N-C@Ru electrolyzer

In order to calculate the electrochemically active surface area (ECSA), the cyclic voltammetry test was executed with the different scan rate (Figure 36a). Double layer capacitance (C_{dl}) of CoSA-N-C@Ru calculated through CV was very high value of 1002 mF cm^{-2}, due to the abundant active sites of the highly porous carbon fibers electrode (Figure 36b).

조선대학교
CHOSUN UNIVERSITY

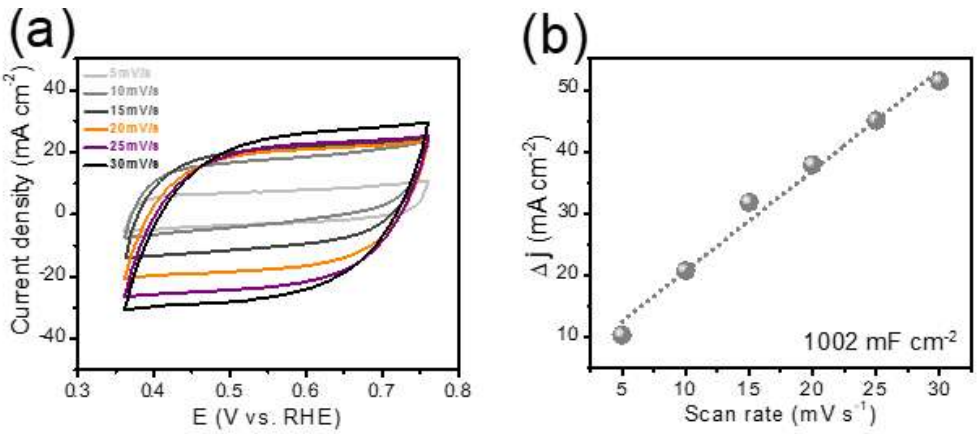

Figure 36. (a) CV curves of CoSA-N-C@Ru with different scan rates, and (b) corresponding double layer capacitance (C_{dl}).

조선대학교
CHOSUN UNIVERSITY

For the durability test of the monolithic catalyst, a current of 10 mA per unit area was applied to measure it as a chronoamperometric test, and it was performed more than 100 hours under both alkaline and acidic conditions (Figure 37). As a result, the initial potential was maintained almost the same in both alkaline and acidic conditions, and it is noteworthy that the graphite rod used as the counter electrode may be damaged as the overpotential increases in acidic conditions. Therefore, using as-prepared Ir/C instead of using a graphite rod can prevent the degradation of performance. For additional durability tests, LSV was measured after 10,000 cycles of CV test to compare the performance of CoSA-N-C@Ru. LSV curves measured after 30th and 10,000th cycles of CV tests showed similar activity toward HER for both alkaline and acidic electrolytes as shown in Figure 38a, and 38b. In addition, the nyquist plots in Figure 39a and 39b also show a similar tendency to result of LSV curves, suggesting excellent durability of CoSA-N-C@Ru. After 10,000 cycles of CV test in alkaline and acidic conditions, the morphology of CoSA-N-C@Ru was well maintained similar to the original structure as observing SEM images in Figure 40 and Figure 41, and the Ru nanoparticles on the surface were also maintained well. In addition, the results of the XPS measurement after the durability test in acidic electrolyte were not significantly different from the original XPS spectrums in Figure 42, proving excellent durability in maintaining the original structure well even after a long time of durability test.

조선대학교
CHOSUN UNIVERSITY

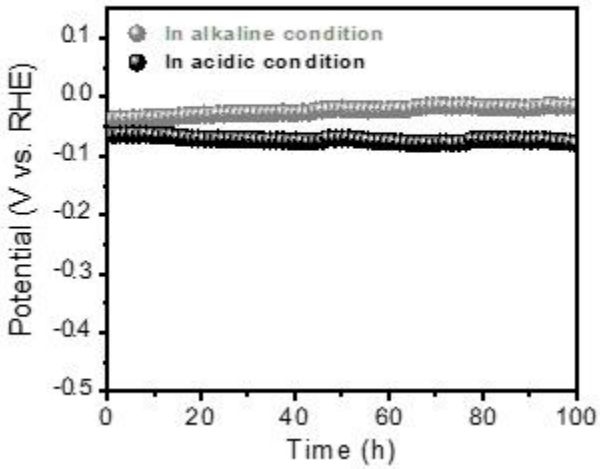

Figure 37. Chronoamperometric test in alkaline and acidic condition.

조선대학교
CHOSUN UNIVERSITY

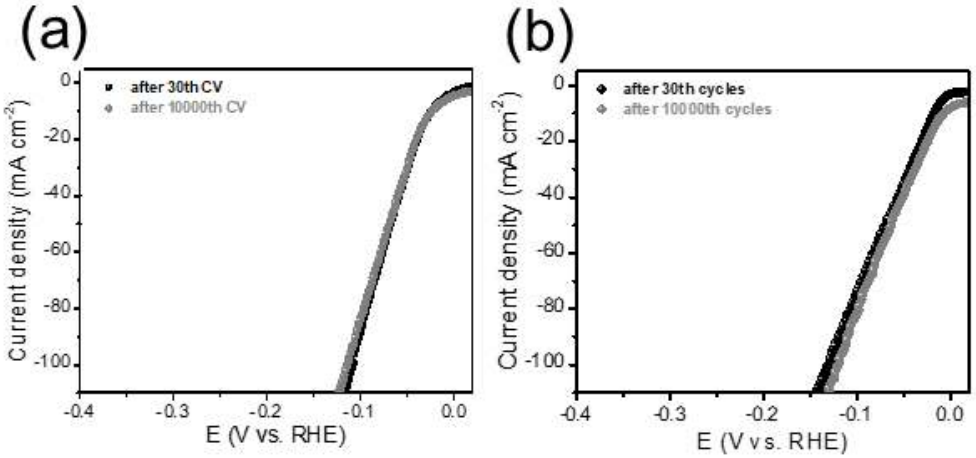

Figure 38. LSV curves after 30th and 10,000th cycles of durability test (a) in an alkaline electrolyte and (b) in an acidic electrolyte.

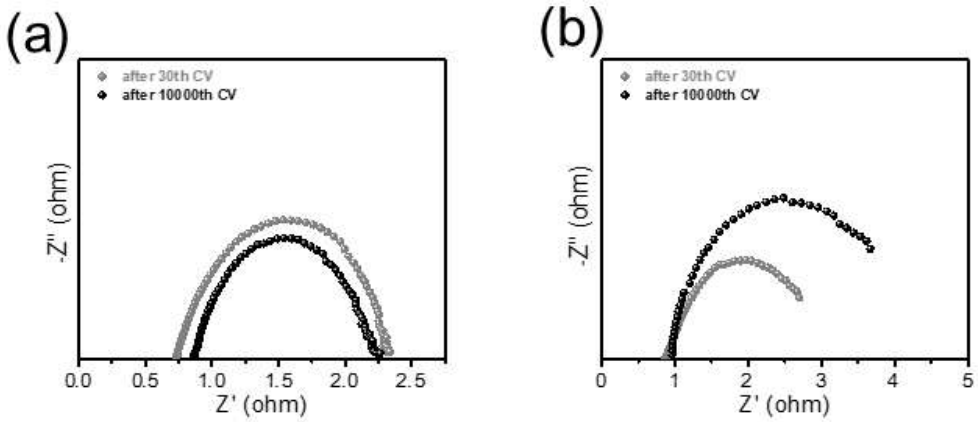

Figure 39. Nyquist plots after durability test (a) in an alkaline electrolyte and (b) in an acidic electrolyte.

조선대학교
CHOSUN UNIVERSITY

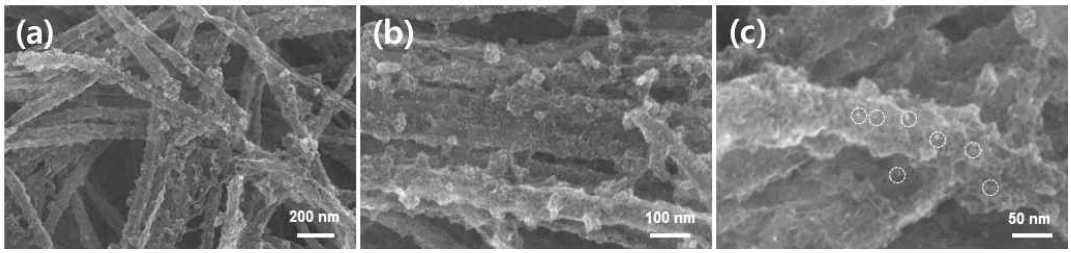

Figure 40. (a-c) SEM images of CoSA-N-C@Ru after durability test for 10,000 cycles in an alkaline condition.

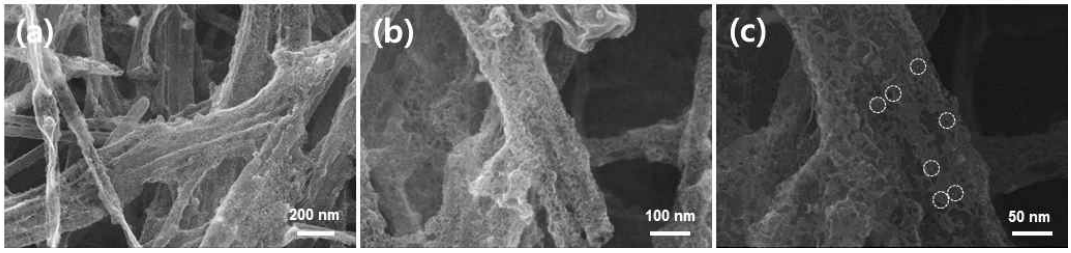

Figure 41. (a-c) SEM images of CoSA-N-C@Ru after durability test for 10,000 cycles in an acidic condition.

조선대학교
CHOSUN UNIVERSITY

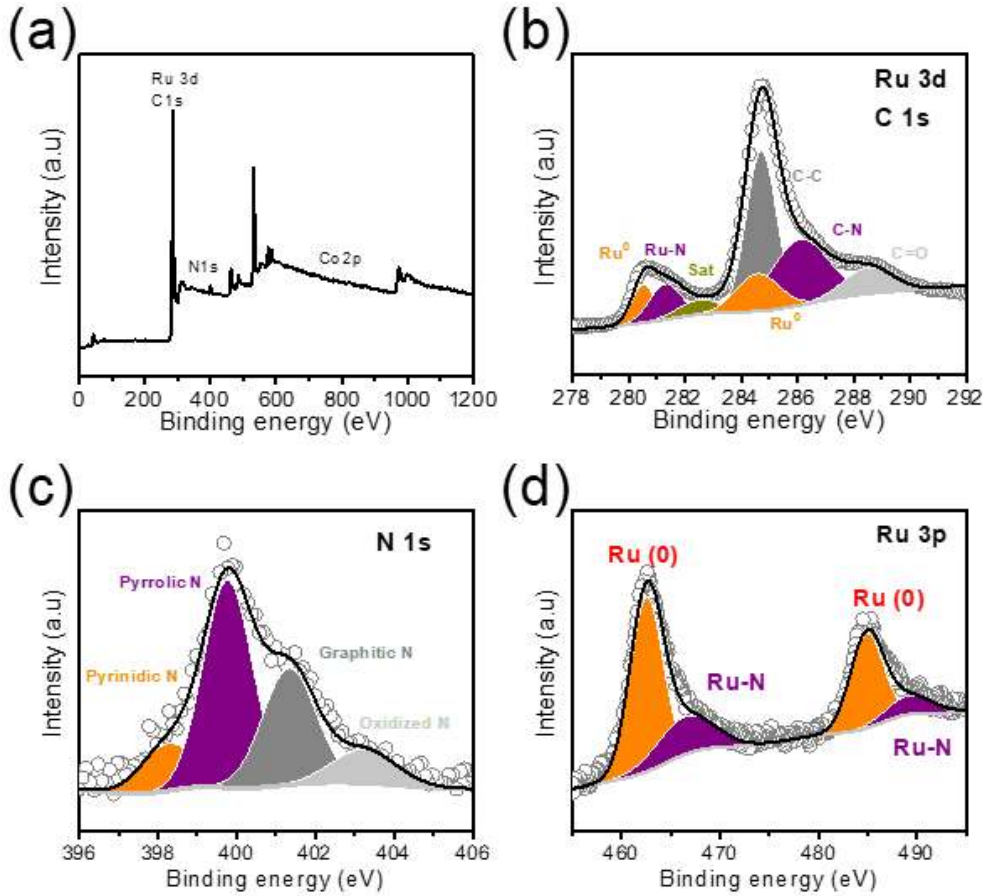

Figure 42. (a) XPS survey spectrum, and fine (b) Ru 3d, (c) N 1s and (d) Ru 3p spectrums of CoSA-N-C@Ru after durability test for 10,000 cycles in an acidic condition.

조선대학교
CHOSUN UNIVERSITY

The oxygen evolution reaction (OER) performance of CoSA-N-C@Ru in acidic electrolyte (0.5 M H_2SO_4) was additionally measured with three-electrode configuration. In OER activities, CoSA-N-C@Ru exhibits the best performance in LSV curves and nyquist plots as depicted in Figure 43a, 43b. Lastly, LSV curves measured through two-electrode configuration which is asymmetric electrolyzer consist of the same monolithic CoSA-N-C@Ru membrane in acidic electrolyte are illustrated in Figure 44 to verify performance for overall water splitting. Compared to the water electrolyzer consisting of Pt/C and IrO_2 (mass loading of 5 mg cm^{-2}), the as-prepared CoSA-N-C@Ru water electrolyzer with ultralow loading of Ru shows superior performance to Pt/C-IrO_2 water electrolyzer toward overall water splitting reaction.

조선대학교
CHOSUN UNIVERSITY

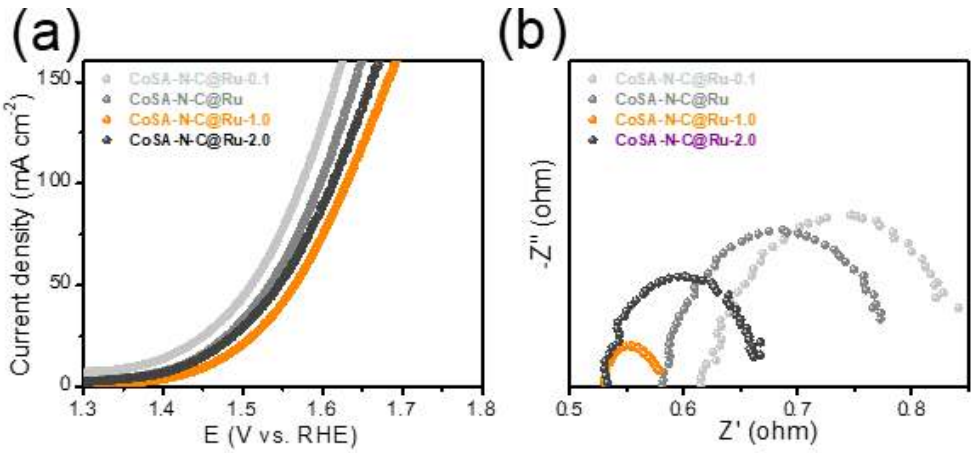

Figure 43. (a) LSV curves, (b) Nyquist plots of CoSA-N-C@Ru-X samples in 0.5 M H_2SO_4 towards OER.

조선대학교
CHOSUN UNIVERSITY

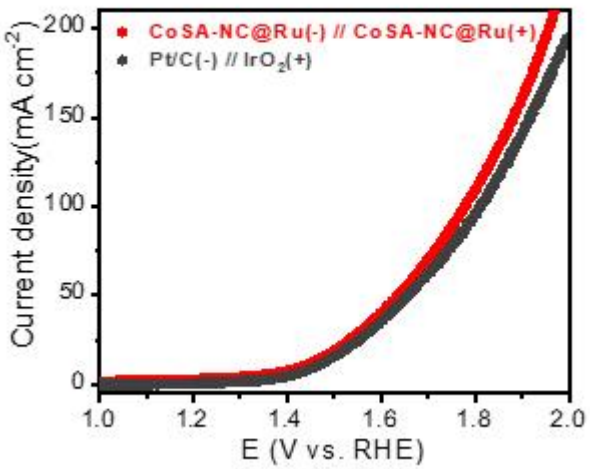

Figure 44. LSV curves of water electrolyzer in 0.5 M H_2SO_4 electrolyte.

조선대학교
CHOSUN UNIVERSITY

IV. Conclusion

In summary, the freestanding monolithic ZnCo-ZIFs is synthesised through self-assembly. And by annealing process, the ZIFs is converted to CoSA-N-C with highly porous structure. During subsequent process of reacting with Ru precursor, finally the CoSA-N-C@Ru is fabricated with ultralow mass loading of Ru which is deposited selectively onto the porous fibers. The HER performance of Co-N-C@Ru in both acidic and alkaline media exhibits comparable results to that of commercial Pt/C. This activity is attributed to the synergistic effect between isolated Co single atoms embedded inside the nitrogen-doped carbon matrix and Ru nanoclusters/nanoparticles anchored to the surface of freestanding monolith. C_{dl} and BET calculations explain the high surface area of porous catalyst and the high performance of HER. This pH-universal activity through HER process is the best among reported literature recently assigned selective deposition which helps to use accessible active fully. Through this work, we present opportunities for new HER catalysts in combination with single metal atoms and metal clusters.

조선대학교
CHOSUN UNIVERSITY

References

[1] Li, J.-S., et al. (2020). "Synergistically enhanced hydrogen evolution reaction by ruthenium nanoparticles dispersed on N-doped carbon hollow nanospheres." Chemical Communications **56**(50): 6802-6805.

[2] Khan, M. A., et al. (2018). "Recent progresses in electrocatalysts for water electrolysis." Electrochemical Energy Reviews **1**(4): 483-530.

[3] Zhu, J., et al. (2019). "Boundary activated hydrogen evolution reaction on monolayer MoS 2." Nature communications **10**(1): 1-7.

[4] Li, X., et al. (2020). "Water splitting: from electrode to green energy system." Nano-Micro Letters **12**(1): 1-29.

[5] Sultan, S., et al. (2019). "Superb water splitting activity of the electrocatalyst Fe 3 Co (PO 4) 4 designed with computation aid." Nature communications **10**(1): 1-9.

[6] Li, K., et al. (2018). "Enhanced electrocatalytic performance for the hydrogen evolution reaction through surface enrichment of platinum nanoclusters alloying with ruthenium in situ embedded in carbon." Energy & Environmental Science **11**(5): 1232-1239.

[7] Zou, X., et al. (2018). "In situ generation of bifunctional, efficient Fe-based catalysts from mackinawite iron sulfide for water splitting." Chem **4**(5): 1139-1152.

[8] Zhao, L., et al. (2018). "Iron oxide embedded titania nanowires−An active and stable electrocatalyst for oxygen evolution in acidic media." Nano Energy **45**: 118-126.

[9] Wang, Z.-L., et al. (2015). "C and N hybrid coordination derived Co−C−N

조선대학교
CHOSUN UNIVERSITY

complex as a highly efficient electrocatalyst for hydrogen evolution reaction." Journal of the American Chemical Society **137**(48): 15070-15073.

[10] Popczun, E. J., et al. (2013). "Nanostructured nickel phosphide as an electrocatalyst for the hydrogen evolution reaction." Journal of the American Chemical Society **135**(25): 9267-9270.

[11] Lu, C., et al. (2017). "Hierarchically structured Cu-based electrocatalysts with nanowires array for water splitting." The Journal of Physical Chemistry C **121**(46): 25875-25881.

[12] Tiwari, J. N., et al. (2018). "Multicomponent electrocatalyst with ultralow Pt loading and high hydrogen evolution activity." Nature Energy **3**(9): 773-782.

[13] Creus, J., et al. (2019). "Ruthenium nanoparticles for catalytic water splitting." ChemSusChem **12**: 2493−2514.

[14] Zhao, Y., et al. (2019). "Ultrathin Rh nanosheets as a highly efficient bifunctional electrocatalyst for isopropanol-assisted overall water splitting." Nanoscale **11**(19): 9319-9326.

[15] Fu, L., et al. (2018). "Ultrathin Ir nanowires as high-performance electrocatalysts for efficient water splitting in acidic media." Nanoscale **10**(4): 1892-1897.

[16] He, T., et al. (2019). "Nanocomposites based on ruthenium nanoparticles supported on cobalt and nitrogen-codoped graphene nanosheets as bifunctional catalysts for electrochemical water splitting." ACS applied materials & interfaces **11**(50): 46912-46919.

[17] Li, M., et al. (2019). "Single-atom tailoring of platinum nanocatalysts for high-performance multifunctional electrocatalysis." Nature Catalysis **2**(6): 495-503.

조선대학교
CHOSUN UNIVERSITY

[18] Fan, Z., et al. (2020). "Highly efficient water splitting over a RuO 2/F-doped graphene electrocatalyst with ultra-low ruthenium content." Inorganic Chemistry Frontiers **7**(11): 2188-2194.

[19] Yuan, S., et al. (2019). "A universal synthesis strategy for single atom dispersed cobalt/metal clusters heterostructure boosting hydrogen evolution catalysis at all pH values." Nano Energy **59**: 472-480.

[20] Chen, D., et al. (2020). "Ultralow Ru loading transition metal phosphides as high -efficient bifunctional electrocatalyst for a solar-to-hydrogen generation system." Advanced Energy Materials **10**(28): 2000814.

[21] Wang, D., et al. (2019). "Single-atom ruthenium based catalyst for enhanced hydrogen evolution." Applied Catalysis B: Environmental **249**: 91-97.

[22] Tiwari, J. N., et al. (2019). "High-Performance Hydrogen Evolution by Ru Single Atoms and Nitrided-Ru Nanoparticles Implanted on N-Doped Graphitic Sheet." Advanced Energy Materials **9**(26): 1900931.

[23] Duan, J., et al. (2017). "Ultrathin metal-organic framework array for efficient electrocatalytic water splitting." Nature communications **8**(1): 1-7.

[24] Ma, T., et al. (2020). "Application of MOF-based materials in electrochemical sensing." Dalton Transactions **49**(47): 17121-17129.

[25] Lu, X. F., et al. (2020). "Metal⁻organic frameworks based electrocatalysts for the oxygen reduction reaction." Angewandte Chemie **132**(12): 4662-4678.

[26] Hall, J. N. and P. Bollini (2019). "Structure, characterization, and catalytic

조선대학교
CHOSUN UNIVERSITY

properties of open-metal sites in metal organic frameworks." Reaction Chemistry & Engineering **4**(2): 207-222.

[27] Bhalothia, D., et al. (2020). "Recent advancements and future prospects of noble metal-based heterogeneous nanocatalysts for oxygen reduction and hydrogen evolution reactions." Applied Sciences **10**(21): 7708.

[28] Ahn, S. H., et al. (2017). "“Wiring” Fe-Nx-Embedded porous carbon framework onto 1D nanotubes for efficient oxygen reduction reaction in alkaline and acidic media." Advanced Materials **29**(26): 1606534.

[29] Kweon, D. H., et al. (2020). "Ruthenium anchored on carbon nanotube electrocatalyst for hydrogen production with enhanced Faradaic efficiency." Nature communications **11**(1): 1-10.

[30] Zheng, B., et al. (2020). "pH universal Ru@ N-doped carbon catalyst for efficient and fast hydrogen evolution." Catalysis Science & Technology **10**(13): 4405-4411.

[31] Lu, B., et al. (2019). "Ruthenium atomically dispersed in carbon outperforms platinum toward hydrogen evolution in alkaline media." Nature communications **10**(1): 1-11.

[32] Zhu, L., et al. (2017). "Synthesis of Ru/CoNi crystals with different morphologies for catalytic hydrogenation." CrystEngComm **19**(25): 3430-3438.

[33] Li, F., et al. (2017). "Efficient extraction and separation of palladium (Pd) and ruthenium (Ru) from simulated HLLW by photoreduction." Separation and Purification Technology **182**: 9-18.

[34] Wang, X., et al. (2019). "One-step synthesis of nitrogen-doped hydrophilic mesoporous carbons from chitosan-based triconstituent system for drug release."

조선대학교
CHOSUN UNIVERSITY

Nanoscale research letters **14**(1): 1-12.

[35] Guo, C., et al. (2019). "A highly nanoporous nitrogen-doped carbon microfiber derived from bioresource as a new kind of ORR electrocatalyst." Nanoscale research letters **14**(1): 1-11.

[36] Yan, Y., et al. (2018). "Ruthenium Incorporated Cobalt Phosphide Nanocubes Derived From a Prussian Blue Analog for Enhanced Hydrogen Evolution." Frontiers in chemistry **6**: 521.

[37] Wang, H., et al. (2020). "Ru and RuO x decorated carbon nitride for efficient ammonia photosynthesis." Nanoscale **12**(23): 12329-12335.

[38] Patil, V., et al. (2016). "Ru-imidazolium halide ionanofluids: synthesis, structural, morphological and thermophysical properties." Journal of Nanofluids **5**(2): 191-208.

[39] Wang, Y., et al. (2020). "Mn 3 O 4/Co (OH) 2 cactus-type nanoarrays for high-energy-density asymmetric supercapacitors." Journal of Materials Science **55**(2): 724-737.

[40] Lu, J., et al. (2019). "Cobalt nanoparticles embedded into N-doped carbon from metal organic frameworks as highly active electrocatalyst for oxygen evolution reaction." Polymers **11**(5): 828.

[41] Su, P., et al. (2021). "Exceptional electrochemical HER performance with enhanced electron transfer between Ru nanoparticles and single atoms dispersed on carbon substrate." Angewandte Chemie.

[42] Chai, L., et al. (2020). "Stringing bimetallic metal–organic framework-derived cobalt phosphide composite for high-efficiency overall water splitting." Advanced Science **7**(5): 1903195.

조선대학교
CHOSUN UNIVERSITY

[43] Qiao, Y.-j., et al. (2021). "A chain-like compound of Si@ CNT nanostructures and MOF-derived porous carbon as an anode for Li-ion batteries." International Journal of Minerals, Metallurgy and Materials **28**(10): 1611-1620.

[44] Morales-Guio, C. G., et al. (2014). "Nanostructured hydrotreating catalysts for electrochemical hydrogen evolution." Chemical Society Reviews **43**(18): 6555-6569.

[45] Xu, J., et al. (2018). "Boosting the hydrogen evolution performance of ruthenium clusters through synergistic coupling with cobalt phosphide." Energy & Environmental Science **11**(7): 1819-1827.

[46] Pu, Z., et al. (2017). "RuP2-based catalysts with platinum-like activity and higher durability for the hydrogen evolution reaction at all pH values." Angewandte Chemie International Edition **56**(38): 11559-11564.

[47] Mahmood, J., et al. (2017). "An efficient and pH-universal ruthenium-based catalyst for the hydrogen evolution reaction." Nature nanotechnology **12**(5): 441-446.

[48] Zheng, Y., et al. (2016). "High electrocatalytic hydrogen evolution activity of an anomalous ruthenium catalyst." Journal of the American Chemical Society **138**(49): 16174-16181.

[49] Wang, J., et al. (2018). "Highly uniform Ru nanoparticles over N-doped carbon: pH and temperature-universal hydrogen release from water reduction." Energy & Environmental Science **11**(4): 800-806.

[50] Hu, C., et al. (2021). "Partial-Single-Atom, Partial-Nanoparticle Composites Enhance Water Dissociation for Hydrogen Evolution." Advanced Science **8**(2): 2001881.